1. INTRODUCTION

1.1. Elongation Factor Tu (EF-Tu)

1.1.1 Structure of Elongation Factor Tu (EF-Tu)

EF-Tu is a member of GTP binding protein superfamily which consists of proteins carrying information and biological components in cells. The common property of the members of this superfamily is; cycling between active and inactive conformations depending on the bound nucleotide either GTP (active) or GDP (inactive). In cells, EF-Tu is an essential protein in protein synthesis transporting amino acyl transfer RNAs (aa-tRNAs) to the amino acyl site of ribosomes.

EF-Tu from bacteria and its eukaryotic/archeal counterpart is a monomeric protein with molecular weight of 40 – 50 kDa. It consists of 3 domains and about 400 amino acids (Figure 1.1). Domain I (aa:1-212) contains a GTP/GDP binding site and Domain II and Domain III consist of aa 212-310 and 310-405 respectively. In this study, the amino acids numbering is done according to the bacterial specie *Thermus aquaticus* unless otherwise stated.

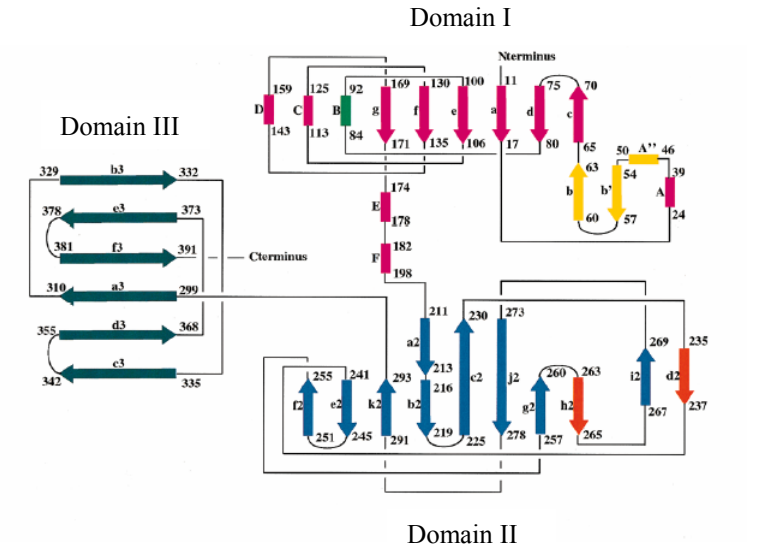

Figure 1.1. EF-Tu of *E.coli* (arrows;βstrands, rectangles; α helices)

Domain I is composed of a core of 6 β strands connected by loops and surrounded by 6 α helices, a fold shared by all GTP binding proteins (GBPs). The nucleotide (GTP) binding pocket in Domain I contains three GBP consensus sequences (GBP I-II-III) and two conserved motifs for prokaryotic elongation factors (EF I-II). The structures in guanine nucleotide binding pocket that are drastically modified by the type of bound nucleotide are called Switch 1 and Switch 2 regions (Figure 1.2). *In vivo*, nucleotides bind to EF-Tu always in the presence of Mg^{+2} that is coordinated to the β and γ phosphates of GTP or α and β phosphates of GDP. In addition to this, each of consensus motifs I and II and the Switch 1 region contains a residue involved in the coordination of the Mg^{+2} bound to the of the nucleotide.

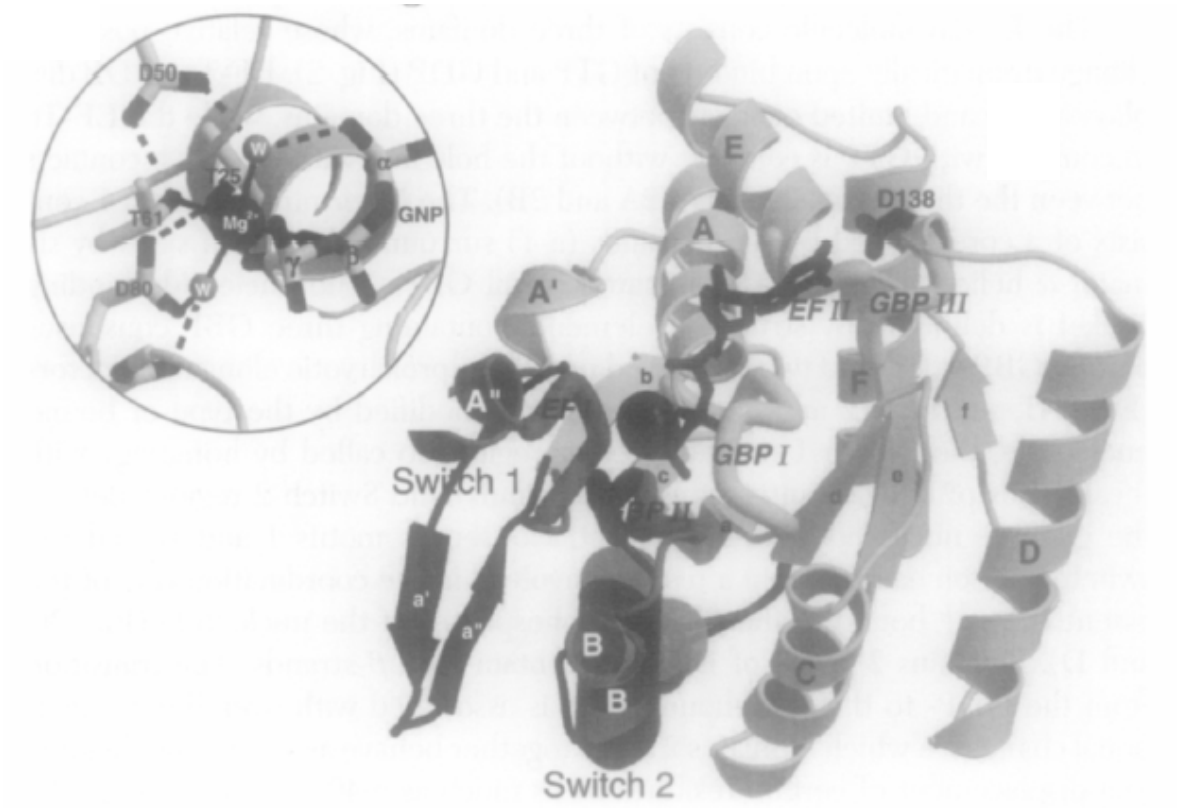

Figure 1.2. Tertiary structure of EF-Tu along with Mg^{+2} coordination

Domains II and III consist of only β strands and in all known structures these two domains are held together in the same relative orientation. As a result of this, the Domains II and III behave as a rigid unit during the functioning cycle of the protein [1].

The available information from structural studies reveal that EF-Tu undergoes a drastic conformational change between its active and inactive forms when bound to GTP and GDP, respectively. As stated above, EF-Tu consists of two movably coupled halves: Domain I that contains the GTP binding site and the block of joint domains II and III. In the absence of GTP, EF-Tu is in a loose or open conformation where the two halves are more or less apart and movable [2] (Figure 1.3).

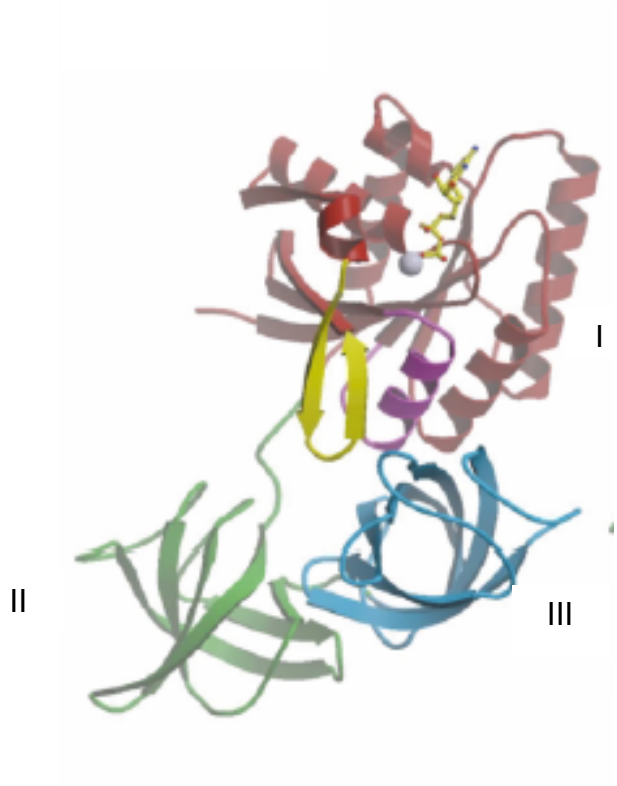

Figure 1.3. GDP (or off-state) conformation of EF-Tu

When a molecule of GTP binds to Domain I of EF-Tu, it induces some local rearrangements in Domain I through the interaction of its γ phosphate group with the nearby atoms at the binding site. These rearrangements result in further conformational changes in the interface region of Domain I facing the joint Domains of II and III. As a consequence of these, a stronger interaction between Domain I and Domain II is provided that draws the two halves of the protein together. This state of EF-Tu is called as the closed or tight conformation [3] (Figure 1.4).

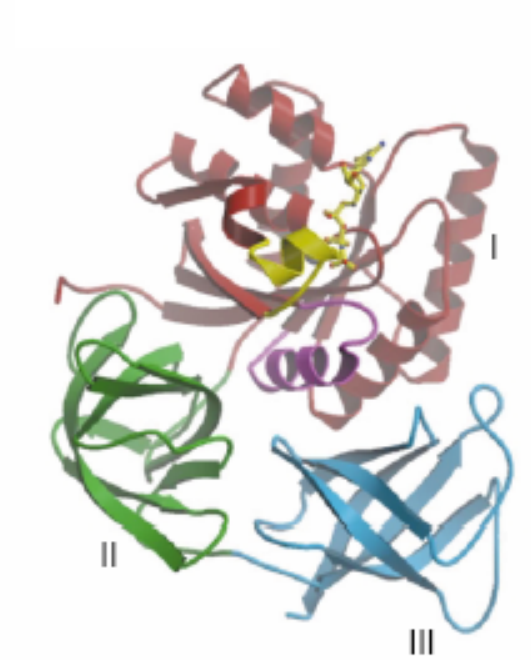

Figure 1.4. GTP (or on-state) conformation of EF-Tu

The closeness of domains exposes a new strong binding site for another ligand of EF-Tu; namely amino acyl transfer RNA (aa-tRNA). aa-tRNA binds to EF-Tu only in the presence of GTP as it requires the formation of the EF-Tu:GTP binary complex that ensures the specific interactions between aa-tRNA and the closed or tight conformation of the protein. The EF-Tu:GTP:aa-tRNA structure is called the ternary complex [4] (Figure 1.5).

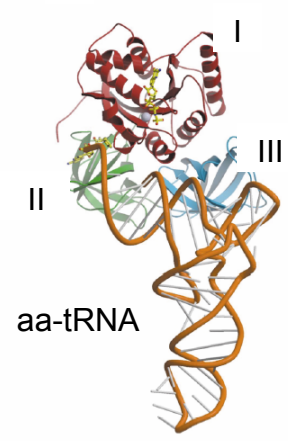

Figure 1.5. EF-Tu:GTP:aa-tRNA (ternary) complex

Formation of a stable EF-Tu:GTP:aa-tRNA ternary complex is essential as the function of EF-Tu:GTP binary complex in bacterial cells is to transport the aa-tRNA to the A site of the mRNA programmed ribosome that carries a peptidyl-tRNA in the P site.

In addition to increased affinity towards aa-tRNA, the binding of a GTP molecule to Domain I induces one more local rearrangement (β to α transition in Swtich 1) that enhances the affinity of EF-Tu to the ribosome. This enables EF-Tu to perform its function of delivering free aa-tRNAs in the cytoplasm to the mRNA programmed ribomes as its GTP (tight) conformation posseses the ability to bind both aa-tRNAs and to the ribosome.

The GTP and GDP conformations of EF-Tu along with the ternary complex structure displays significant conformational changes in the Switch 1 and Switch 2 regions of EF-Tu. The Switch 1 region of EF-Tu (a.a. 52-65) consists of two small α helices in the GTP form; namely A' and A" which are nearly perpendicular to each other (Figure 1.6)

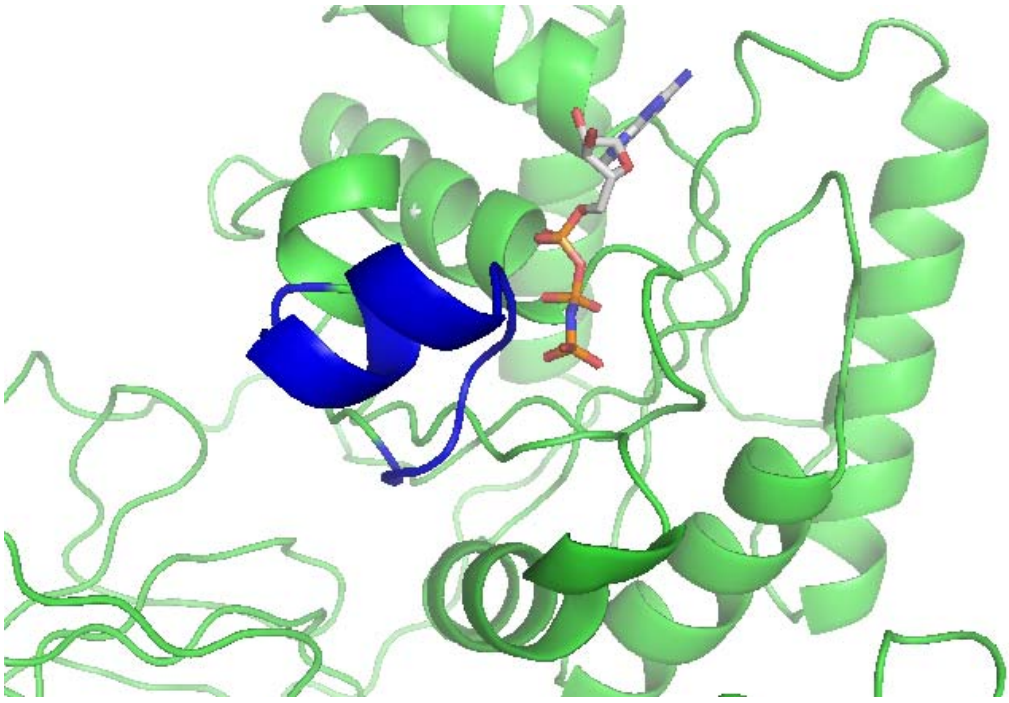

Figure 1.6. Switch 1 region (blue) in GTP conformation of EF-Tu

However, in the GDP form, A" is unwound and a β hairpin is formed whereas the A' remains essentially unchanged (Figure 1.7). In GDP complex, Switch 1 region is placed at the aa-tRNA binding site preventing the interaction of EF-Tu:GDP complex with the aa-tRNA.

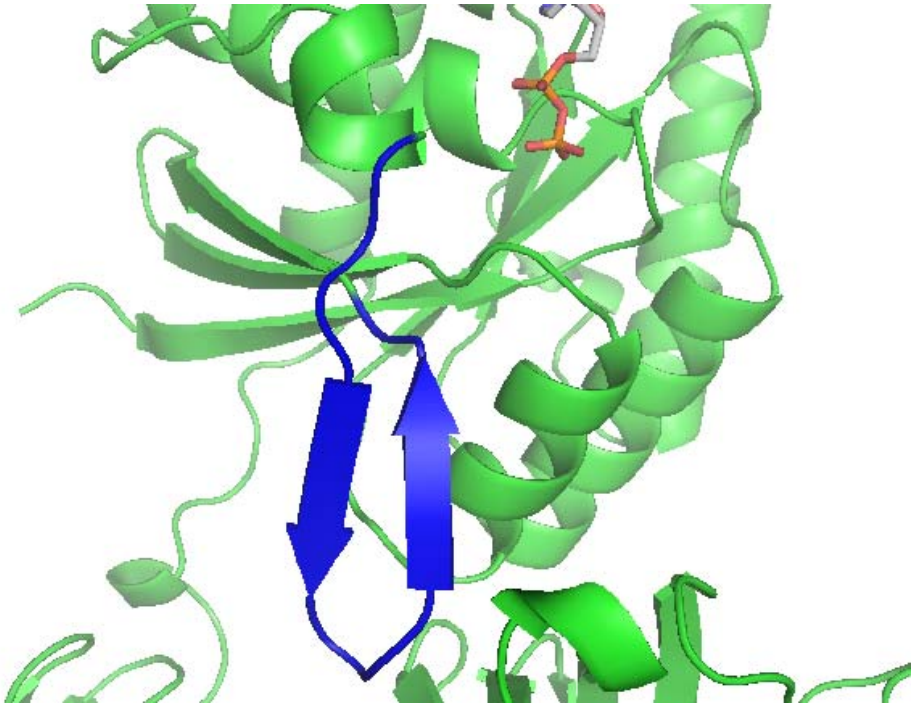

Figure 1.7. Switch 1 region (blue) in GDP conformation of EF-Tu

T62, a conserved residue located in Switch 1 region, is coordinated to Mg^{+2} ion in the GTP form with a distance of 4.3 Å between the C_α of T62 and Mg^{+2} . However, in the GDP form the distance between the C_α of T62 and Mg^{+2} is extended to 16 Å abolishing the interaction. This example displays the significant amount of change in the relative position of Switch 1 region in GTP and GDP forms.

On the other hand, Switch 2 region (aa 82-97) unwinds one helical turn at its C terminus and form another one at the N terminal end while changing from GTP form (Figure 1.8) to the GDP form (Figure 1.9).

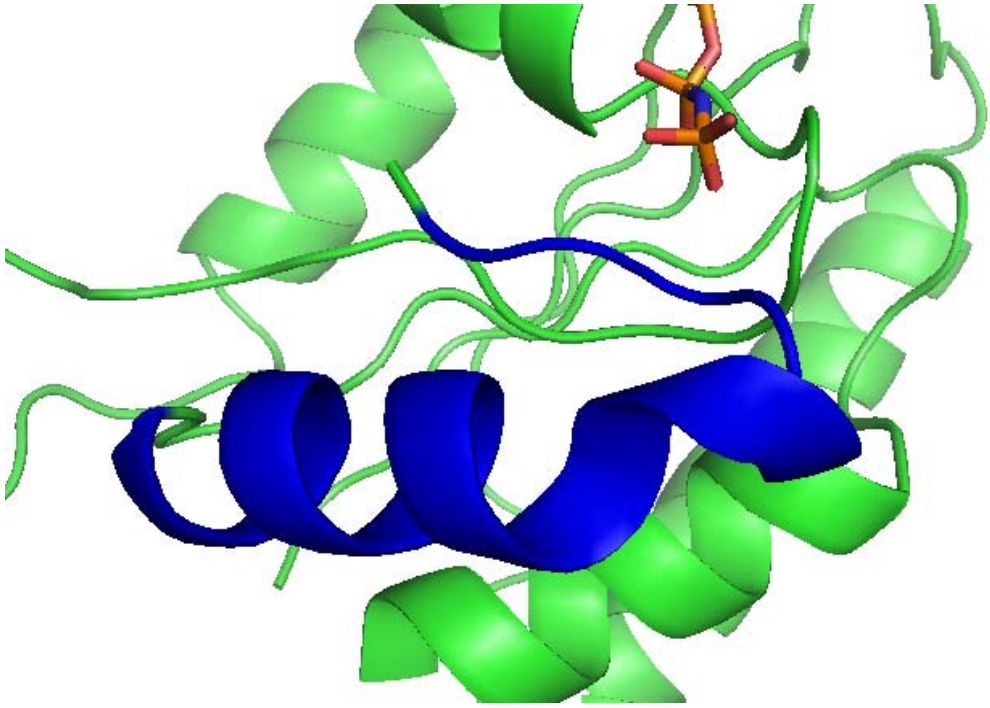

Figure 1.8. Switch 2 region (blue) in GTP conformation of EF-Tu

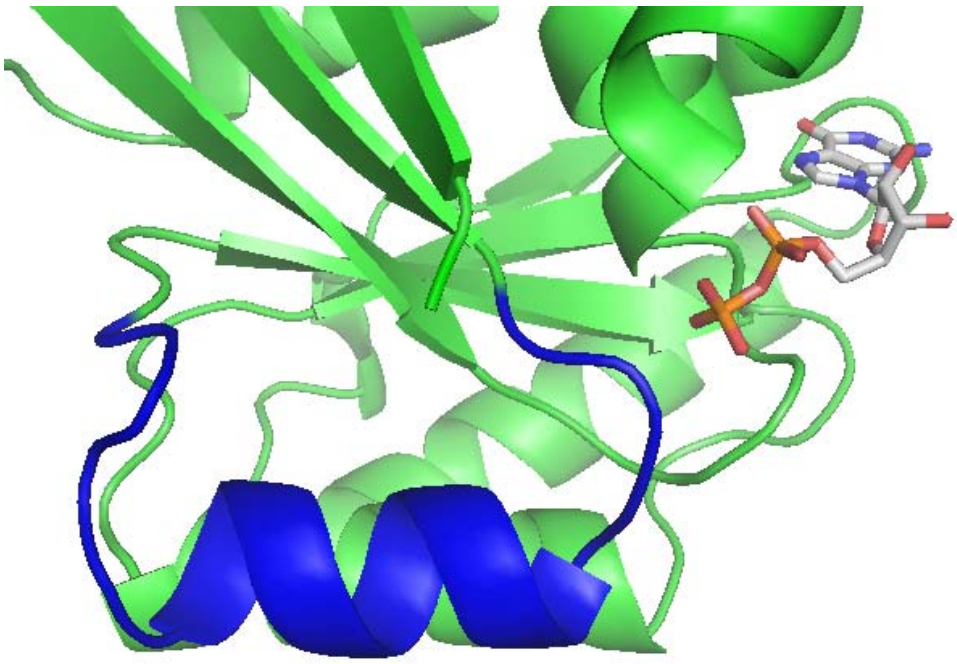

Figure 1.9. Switch 2 region (blue) in GDP conformation of EF-Tu

1.1.2 Elongation Factor Tu (EF-Tu) in Protein Synthesis

When the ternary complex of EF-Tu:GTP:aa-tRNA binds to the ribosome, cognate codon anticodon interaction triggers the fast hydrolysis of the EF-Tu bound GTP. The hydrolysis of GTP leads to a remarkable conformation change in EF-Tu as it returns to the GDP (loose) conformation from its GTP (tight) conformation. This conformational change decreases the affinity of EF-Tu to the ribosome and abolishes the affinity of it towards the aa-tRNA resulting in the release of EF-Tu:GDP complex from aa-tRNA and ribosome.

The net outcome of this functioning cycle of EF-Tu is the delivery of aa-tRNAs to the mRNA programmed ribosomes by means of hydrolysis of EF-Tu bound GTP molecules to the GDP molecules (Figure 1.10).

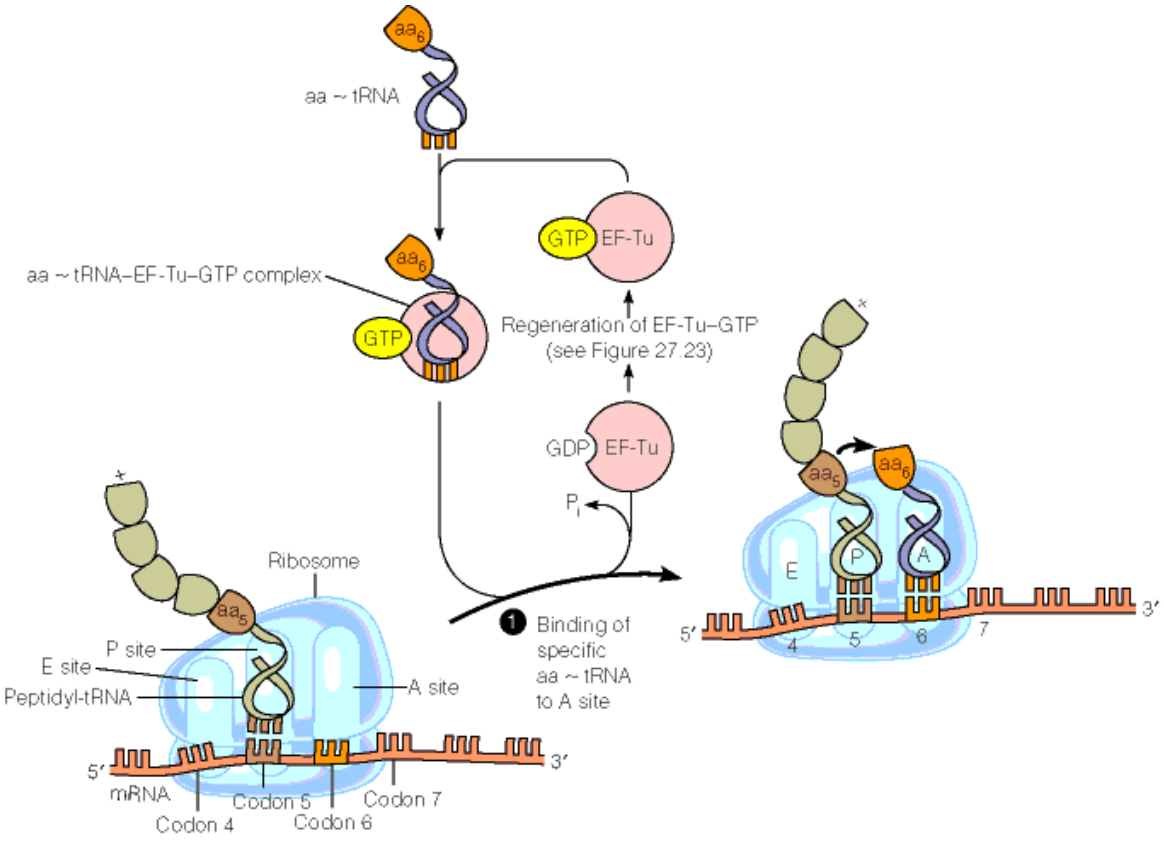

Figure 1.10. The functioning cycle of EF-Tu

EF-Tu has an affinity for GDP which is two orders of magnitude higher than for GTP; therefore organisms need certain mechanisms to convert the EF-Tu:GDP (inactive) complexes to EF-Tu:GTP (active) complexes in order to sustain the proper rate of polypeptide synthesis.

Various factors contribute to the recycling of the released EF-Tu:GDP complexes to EF-Tu:GTP complexes. The first of these factors is the action of nucleotide exchange factors (EF-Ts) on EF-Tu:GDP complexes. The mechanism of GTP – GDP nucleotide exchange by EF-Ts is thought to proceed by destabilizing the EF-Tu guanine nucleotide complex that leads to the release of the present nucleotide from the guanine nucleotide binding site that is replaced by a GTP molecule later.

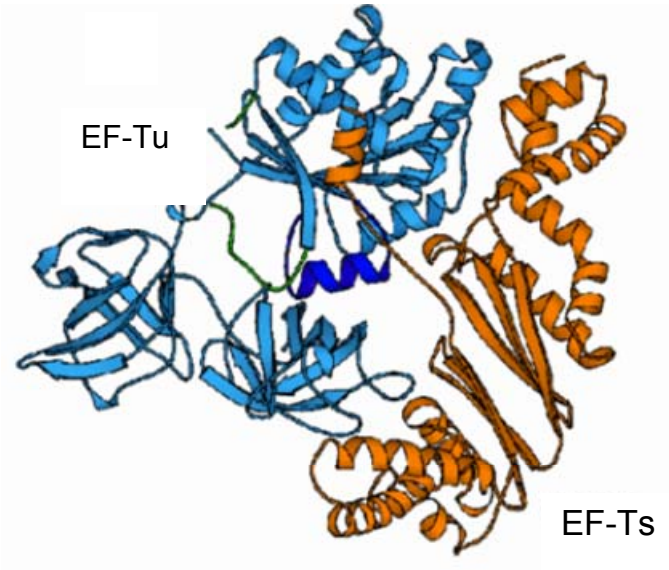

Figure 1.11. EF-Tu:EF-Ts complex

The second factor is the result of interaction of EF-Tu with the aa-tRNA that increases the affinity of EF-Tu to the GTP while decreasing the GTP hydrolysis rate. Another factor is the 5 to 10 fold higher concentration of GTP than that of GDP in the cell. These factors enable cells to sustain a high concentration of EF-Tu:GTP complex to ensure rapid protein biosynthesis on the ribosomes.

Apart from the ribosome induced GTP hydrolysis, EF-Tu has a very low intrinsic GTPase activity. This low intrinsic activity of EF-Tu can be enhanced by monovalent cations, vacant ribosomes and kirromycin, from 5 to 100 fold. Moreover, the strongest enhancer of GTP hydrolysis is a mRNA programmed ribosome with occupied P site. Following the cognate codon anticodon interaction, ribosome induces the GTP hydrolysis of EF-Tu with a rate of 10^5 times faster than that of intrinsic GTPase activity of EF-Tu [5-8].

1.1.3. Mutational Data on Elongation Factor Tu (EF-Tu)

Significant amount of mutational data is present on EF-Tu and a considerable amount of it is about the amino acid residues forming the nucleotide binding pocket located in Domain I. Among these mutational data, of special importance are the ones concerning the magnesium coordination network as the mutations of these residues affect both the affinity of EF-Tu towards GTP or GDP and the GTPase activity of EF-Tu.

The residues forming the magnesium ion coordination in *Thermus aquaticus* are; Threonine 25 (T25) and Threonine 62 (T62) that directly bind the magnesium ion via the oxygen (O) atom of their hydroxyl (OH) group and, Aspartate 51 (D51) and Aspartate 81 (D81) each of which has hydrogen bonds to one water molecule in the coordination sphere of magnesium ion. In addition to these, magnesium ion is coordinated one oxygen atom from each of the β and γ phosphates group of the GTP molecule (Figure 1.12).

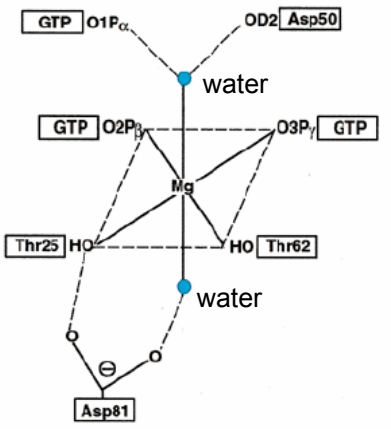

Figure 1.12. Magnesium coordination in EF-Tu:GTP

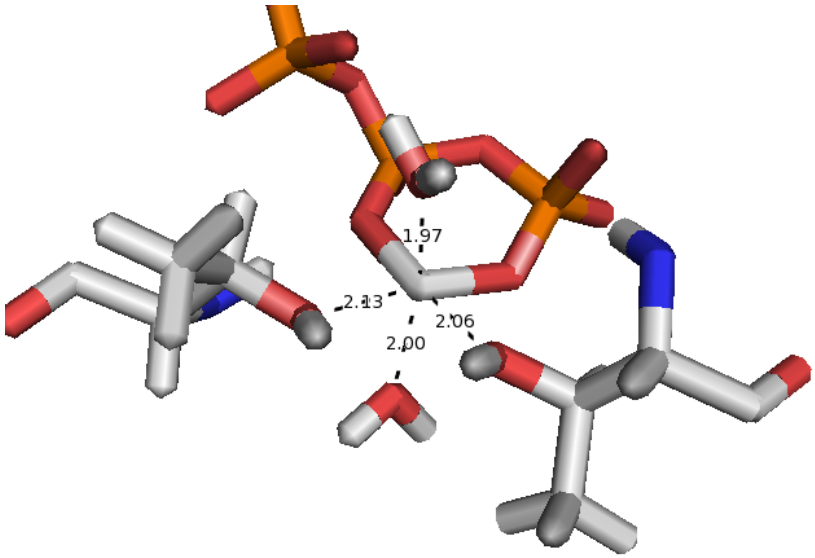

Figure 1.13. Magnesium coordination in EF-Tu:GTP (T25,T62,H_2O)

D51 and D81 residues make hydrogen bonds with hydroxyl groups of T62 and T25 respectively in addition to their hydrogen bonds with water molecules coordinated to the Mg^{+2} ion [5].

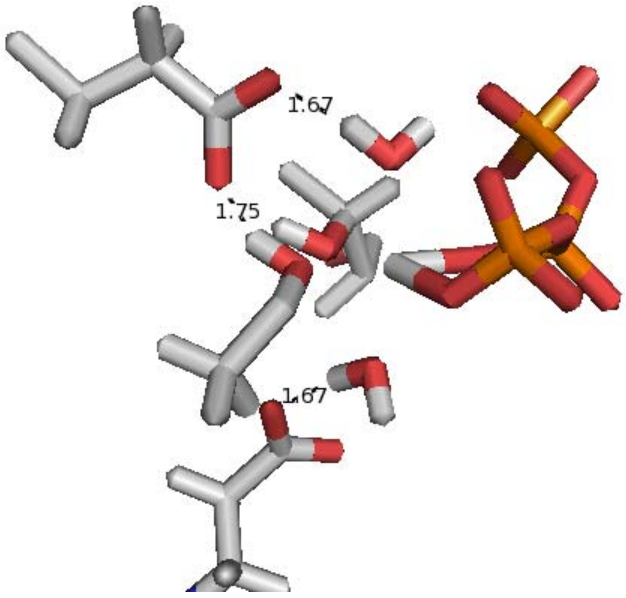

Figure 1.14. Magnesium coordination in EF-Tu:GTP (T25, D51,T62,D82,H_2O)

In one experimental study [9], the invariant T62 in the effector region (Switch 1) of *Thermus thermophilus* EF-Tu was substituted to serine (T62S) and alanine (T62A) residues by means of site directed mutagenesis. The EF-Tu T62S variant displayed similar properties with respect to thermostability, amino acyl-tRNA binding, GTPase activity and *in vitro* translations as the wild type whereas the T62A variant displayed impaired ability for polypeptide synthesis with a very low intrinsic and ribosome induced GTPase activity. These results are in agreement with the assumption that T62 is interacting with the Mg^{+2} ion, γ phosphate of GTP and a water molecule that is involved in GTP hydrolysis [9] (Figure 1.15).

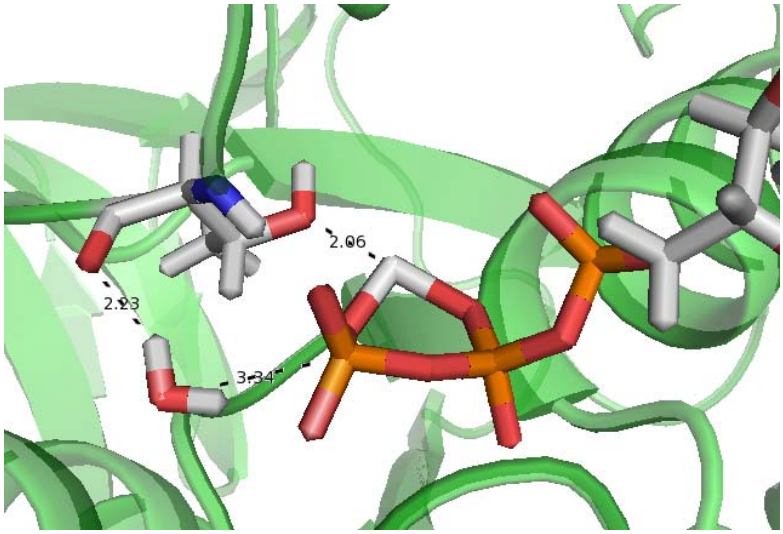

Figure 1.15. T62 coordination with Mg^{+2} and attacking H_2O molecule

In another experimental study [10] D80 (D81 in *Thermus aquaticus*) residue of *Escherichia coli* was substituted to an asparagine (D80N) that results in a dramatic decrease in affinity of mutant EF-Tu to GDP molecules along with a decreased intrinsic GTPase activity while the ribosome induced GTP hydrolysis is stimulated to the same rate as wild types in the presence of empty ribosomes i.e. by a factor of 88. The lack of a negative charge attracting Mg^{+2} in D80N probably leads to a weaker bonding and the perturbation of the Mg^{+2} interaction by this way probably results in a decrease in intrinsic GTPase activity. Although D80 seems to be involved in the tight regulation of GTPase, its mutation to asparagine residue does not preclude the activation by ribosome [10].

Histidine 84 (H85 in *Thermus aquaticus*) mutations constitute another important class of EF-Tu mutations that provide a wealth of information about the mechanism of intrinsic and ribosome induced GTP hydrolysis on EF-Tu. Crystal structures of several Ras-like and heterotrimeric GTP binding proteins indicated that a glutamine residue is crucial for the stabilization of GTPase transition state by correct positioning of both the water molecule and the γ phosphate. Ras-like and heterotrimeric G proteins -two important class of G proteins with similar GTP binding sites like in EF-Tu- contain a conserved glutamine residue that was studied extensively; both experimentally and theoretically. In analogy with the glutamine residue in Ras-like and heterotrimeric G proteins, H84 of EF-Tu was suggested to perform a similar role in the intrinsic and ribosome induce GTP hydrolysis of EF-Tu.

In an experimental study [11], H84 of *Escherichia coli* was substituted to glutamine (H84Q) and alanine (H84A) to investigate the catalytic activity of it in the GTP hydrolysis reaction. The intrinsic GTPase activity of EF-Tu is reduced to 35% in the H84Q mutant whereas only 10% of GTPase activity was observed in H84A mutant.

Upon ternary complex binding to poly(U) programmed ribosomes, the rate of GTP hydrolysis was moderately reduced by histidine substitution to glutamine in EF-Tu from *E.coli* or *T. thermophilus* (12 fold). On the other hand, the replacement of histidine to alanine decreased the rate of GTP hydrolysis by more than six orders of magnitude, which translates into an increase in the activation energy barrier by 8.36 kcal/mol. A closer kinetic investigation of the GTP hydrolysis in H84A mutant led to the result that only the GTP hydrolysis step was slowed extensively whereas the other elemental steps like A site binding are little affected. These results indicate that H84 has a catalytic effect on the ribosome induced GTP hydrolysis of EF-Tu whereas its effect is not substantial in the intrinsic GTPase activity.

One explanation to the catalytic effect of H84 in the GTP hydrolysis reaction is a general base mechanism in which histidine abstracts a proton from the attacking water molecule resulting in the formation of a hydroxide ion (Figure 1.16). Hydroxide ion is a better nucleophile than a water molecule so the nucleophilic attack to the phosphorus atom of γ phosphate will be easier. However, recent studies on the GTPase activation and

GTPγS hydrolysis show no dependence on pH which is at variance with the expected behavior if a general base with a pK_a of 7 such as Histidine were involved in catalysis.

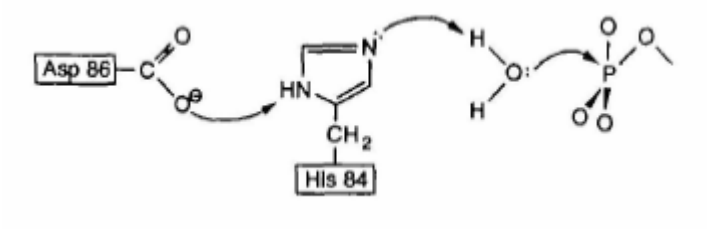

Figure 1.16. General base mechanism for histidine 84

The most realistic explanation proposes that the catalytic role of H84 is to form hydrogen bonds to the attacking water and γ phosphate to precisely align the groups directly involved in the reaction that is in accordance with the similar role of conserved glutamine residues in Ras-like and heterotrimeric G proteins [11-12] (Figure 1.17).

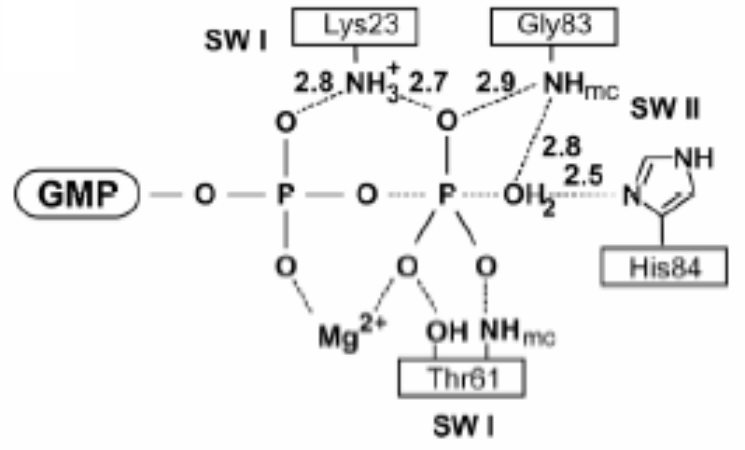

Figure 1.17. Histidine 84 aligning attacking water molecule

In addition to these, it was proposed that a hydrophobic barrier formed by Valine 20 (V20) and Isoleucine 60 (I60) prevents the free rotation of H84 to the active site. The side chain of H84 is normally directed towards the solvent and this barrier can prevent the free rotation of it towards the active site thereby inhibiting the undesired elevated rates of intrinsic GTPase activity. However, neither substitution valine to glycine (V20G) [13] nor

isoleucine to alanine (I60A) [10] increases the EF-Tu GTP hydrolysis, in contrast to prediction that the intrinsic GTP hydrolysis rate should increase with a reduction in the hydrophobic barrier.

An important experimental study [14] sheds light on the role of Arginine 58 (R59 in *Thermus aquticus*) on the GTPase activity of EF-Tu and on the binding of aa-tRNA to the EF-Tu. In order to investigate these properties, R58 was substituted to alanine (R58A) and glutamic acid (R58E). The intrinsic GTPase activities of R58A and R58E mutants remained the same in comparison to the wild types indicating that R58 is not an important factor for this reaction. The GTPase activity in the presence of programmed ribosomes revealed that R58 does not possess a catalytic role in the ribosome induced GTPase activity but it is probably involved in the binding of EF-Tu to the ribosome.

In addition to these it was observed that R58 mutations did not alter the affinity of EF-Tu to the guanine nucleotides but it was also found that R58 was involved in the binding of aa-tRNA to the EF-Tu although it didn't seem to have a stabilizing effect on amino acyl of amino acyl bond.

In the same experimental study, aspartate 86 (D87 in *Thermus aquaticus*) was mutated to alanine (D86A), asparagine (D86N) and glutamic acid (D86E) in order to investigate the possible roles of D86 in the GTPase activity of EF-Tu and in the binding of aa-tRNA to the EF-Tu.

The results obtained using these mutant EF-Tus indicated that D86 is not essential for the binding of aa-tRNA while it seems that it is crucial for the binding of both guanine nucleotides; GTP and GDP. D86 was also found to be involved in the intrinsic GTPase activity of EF-Tu but probably it is not an essential part of it. Moreover, the precise definition of the role of D86 in GTPase activity is still lacking [14].

1.2. Phosphate Hydrolysis Mechanism

As the hydrolysis of GTP to GDP is of central importance in the functioning cycle of G proteins, considerable amount of computational and experimental studies were directed to elucidate the mechanism of non-enzymatic phosphate hydrolysis in solution.

The computational studies on phosphate hydrolysis reactions can be classified according to their substrates (methyl monophosphate, methyl diphosphate, GTP etc.) and protonation states, their system definition (presence or absence of Mg^{+2}, gas or solvent phase etc.) and their computational methods (DFT, QM/MM optimization or simulation etc.). The differences in the perspectives of these studies provided a wealth of information on the different aspects of the phosphate hydrolysis problem.

Beyond all these classifications of studies, the main mechanistic debate on GTP hydrolysis or phosphate hydrolysis in general is whether it follows an associative or dissociative pathway (Figure 1.18).

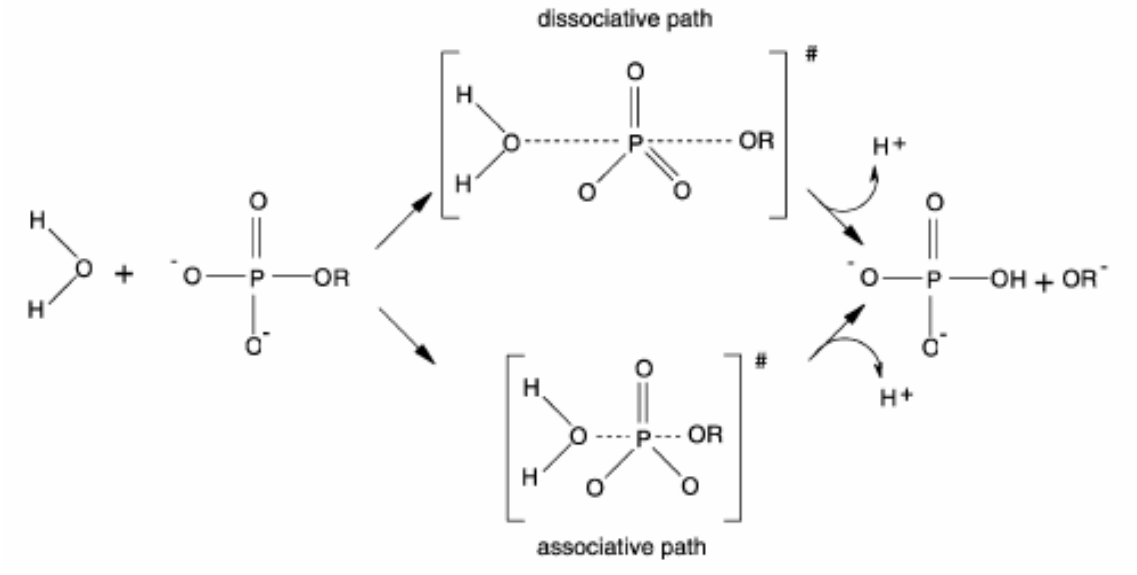

Figure 1.18. Associative vs dissociative pathway

The associative pathway can be described by the formation of an intermediate with a penta-coordinated phosphorus atom whereas the dissociative pathway can be described by the formation of a metaphosphate ion as an intermediate. However, these are the extreme cases and when a mechanism is considered it is usually the associative or dissociative character of the mechanism rather than a complete associative or dissociative pathway. The character of the mechanism can be identified by investigating the γ phosphorus – oxygen (bridge) and γ (or β depending on substrate) phosphorus – oxygen (water) distances (Figure 1.19).

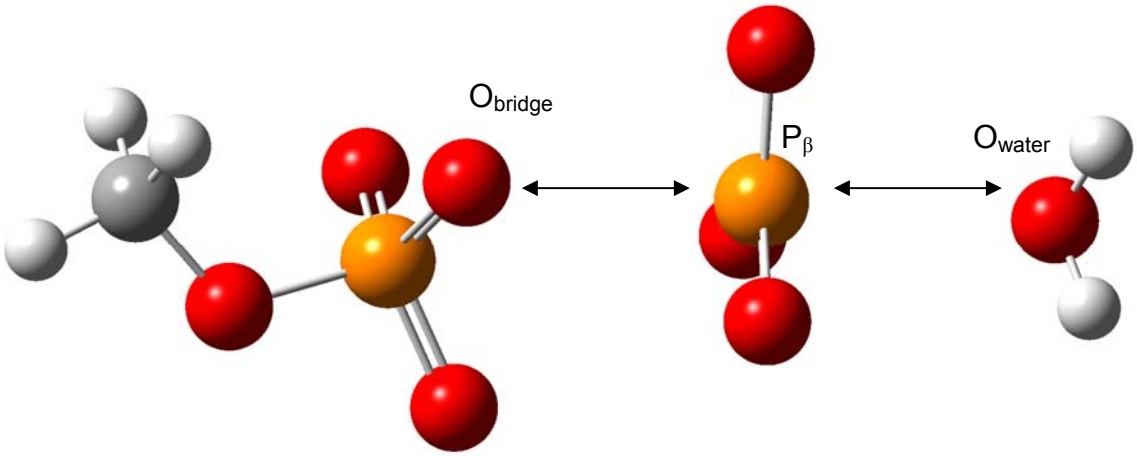

Figure 1.19. Associative vs dissociative character

The experimental studies directed towards the elucidation of phosphate hydrolysis mechanisms provided significant amount of insight about the nature of the transition state of this special reaction. For example, it was found that important amount of negative charge shifts to β phosphate group from the γ phosphate and that metaphoshate is present in aprotic solvents but not observed in protic solvents. Moreover, the nature of the nucleophile and leaving group was shown to be a determining factor for the phosphate hydrolysis mechanism such that an increase in the pK_a value of the nucleophile favors an associative mechanism while an decrease in the pK_a value of the leaving group favors a dissociative mechanism.

In addition to these, $\Delta G_{activation}$ values of 44 kcal/mol [15] and 28 kcal/mol [16] were estimated for monomethyl phosphate dianion ($CH_3OPO_3^{-2}$) and monomethyl pyrophosphate trianion ($CH_3OPO_3PO_3^{-3}$) respectively. Another interesting finding in the studies of phosphate hydrolysis reactions was the non catalytic effect of Mg^{+2} that was challanged by some computational studies later.

The experimental studies using Linear Free Energy Relationships (LFERs), kinetic isotope effects and activation entropies generally pointed out a dissociative pathway for the hydrolysis of phosphate monoesters. However, Warshel and Åqvist investigated the experimental results on phosphate monoester hydrolysis reactions using thermodynamic analysis of observed linear free energy relationships and concluded that associative and concerted mechanisms are consistent with available experimental data as well as dissociative mechanism [17].

On the other hand, Hu and Brinck examined the mechanism for the hydrolysis of the methyl phosphate mono anion using gas phase reaction coordinates and solvation free energies by means of ab initio and density functional theory. Their results indicate that dissociative pathway is more favorable than the associative pathway and that presence of one additional water molecule enhances this preference by forming a six membered ring instead of four membered one [18] (Figure 1.20).

(a) (b)

Figure 1.20. Methyl mono phosphate anion with (a) no H_2O (b) one H_2O

Moreover, Bianciotto *et. al*. studied the mono phosphate mono ester hydrolysis using a dissociative mechanism via polarized continuun models (PCM) and explicit water molecules. The authors proposed the presence of zwitterionic complexes pointing that the

collapse of these zwitterionic complexes consititutes the rate determining step [19]. However, Wang *et. al.* reported these structures as complexes rather than zwitterionic species [20] (Figure 1.21).

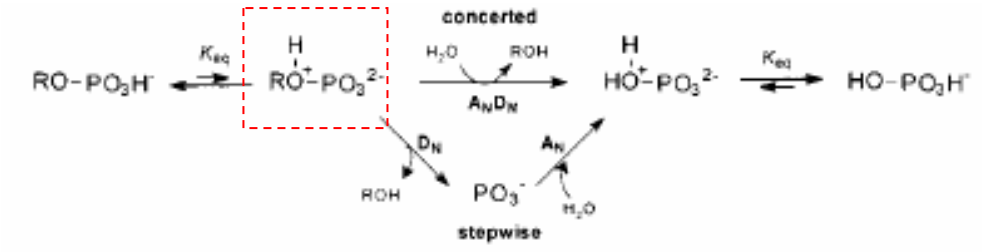

Figure 1.21. Zwitterion pathway proposed by Bianciotto *et. al.*

Wang *et. al.* [20] systematically studied the hydrolysis of mono phosphates and tri-phosphates in gas phase and aqueous solution using hybrid density functional methods. Their results indicate that for mono phosphate ester, the dissociative pathway is much more favorable than the associative pathway. The activation barriers for the associative and dissociative pathways of tri-phosphate hydrolysis are very similar in aquoeus solution, although the dissociative pathway is more favorable in the gas phase.

Klåhn *et. al.* [21] recently investigated the mechanism of hydrolysis of phosphate monoesters and triphosphate anions in solutions and proteins performing calculations ranging from ab initio calculations with implicit solvent models to ab initio QM/MM free energy calculations. It was shown that potential energy surface for the associative and dissociative path is very flat and the relative heights of the reaction barriers of associative and dissociative transition states depend upon the nature of the systems with an increasing dissociative character upon decrease of pK_a of the leaving group. Three distinct transition states (namely; associative, dissociative and concerted) were proposed for the methyl diphosphate system in the presence of Mg^{+2} ion, with dissocative TS being 1 kcal/mol lower than the others (Figure 1.22). Moreover, they studied on the GTPase reaction of Ras–GAP system and found that the lowest transition state is associative.

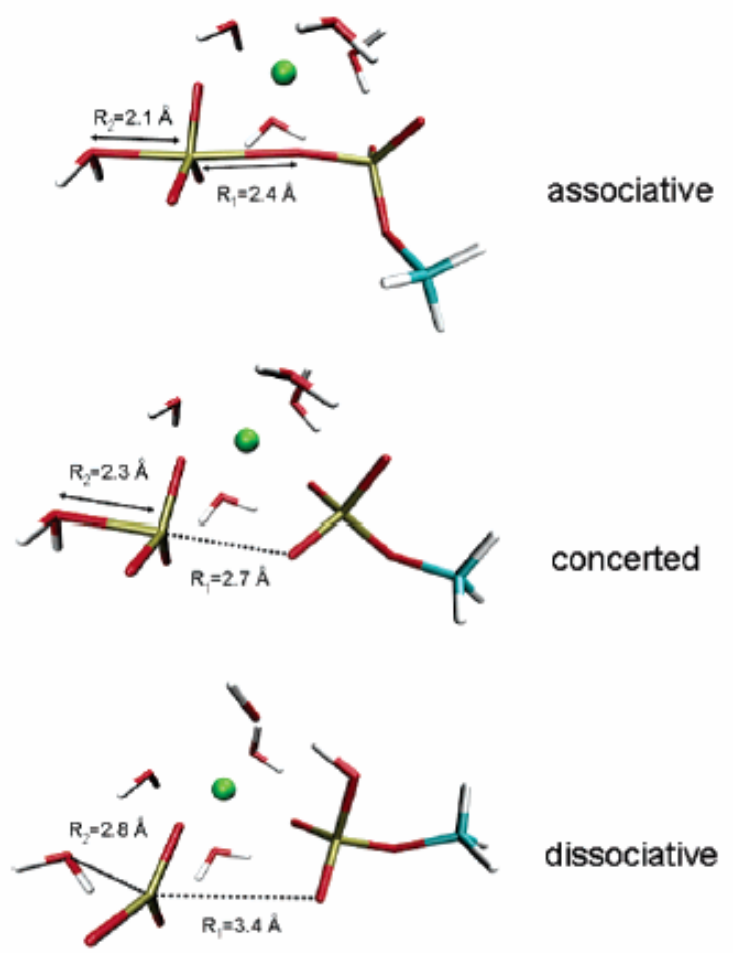

Figure 1.22. Three transition states proposed by Klåhn *et. al*.

In additon to these, there are other theoretical studies in the literature on methyl phosphate and phenyl phosphate hydrolysis [22], catalytic effect of magnesium on phosphate hydrolysis [23] , ATP hydrolysis [24] and GTP hydrolysis mechanism of Ras and Ras like GTPases [25-31].

2. AIM OF THE STUDY

The primary aim of this study is to comprehend the nature of the hydrolysis reaction of methyl pyrophosphate trianion in aqueous solution using quantum mechanical tools. The study covers several aspects of the hydrolysis reaction of methyl pyrosphate trianion ranging from the effect of the Mg^{+2} ion on the hydrolysis reaction to the detailed investigation of the reaction coordinate..

Another important task is the investigation of the GTP conformation of Elongation Factor Tu (EF-Tu) from *Thermus aquaticus* by using molecular dynamics simulations.

3. METHODOLOGY

All the geometry optimizations have been carried out by using the density functional theory (DFT) [32, 33]. Harmonic frequencies have been computed in order to identify the stationary points as minima or transition states (with imaginary frequencies) and to obtain thermal energy and entropy contributions. For some transition states, intrinsic reaction coordinate (IRC) calculations have been carried out to verify the nature of the transition states. For certain geometries loose optimization criteria (max displacement <5000) were used in order to overcome optimization problems. All computations have been carried out by using the Gaussian 03 program [34].

The energetic results are reported as the change in the energy (ΔE), that is the sum of the electronic energy (ΔE_{el}) and free energy of solvation(ΔG_{sol}) for solvent calculations. The ΔE value is calculated from difference between the energies of the products and the reactants ($E_P - E_R$) using reactant complexes. On the other hand, free energies (ΔG) are calculated by means of frequency calculations using seperated reactants rather than complexes.

3.1 Density Functional Theory (DFT)

The density functional theory is based on the Kohn-Hohenberg theorems proposed in 1964. The first theorem states that the electron density $\rho(r)$ determines the external potential $v(r)$, i. e. the potential due to the nuclei. The second theorem introduces the variational principle. Hence, the electron density can be computed variationally and the position of nuclei, energy, wave function and other related parameters can be calculated.

The electron density is defined as:

$$\rho(x) = N \int \ldots \int \left|\Psi(x_1, x_2, \ldots x_n)\right|^2 dx_1 dx_2 \ldots dx_n \qquad (3.1)$$

where x represents both spin and spatial coordinates of electrons.

The electronic energy can be expressed as a functional of the electron density:

$$E[\rho] = \int v(r)\rho(r)dr + T[\rho] + V_{ee}[\rho] \tag{3.2}$$

where $T[\rho]$ is the kinetic energy of the interacting electrons and $V_{ee}[\rho]$ is the interelectronic interaction energy. The electronic energy may be rewritten as:

$$E[\rho] = \int v(r)\rho(r)dr + T_s[\rho] + J[\rho] + E_{xc}[\rho] \tag{3.3}$$

with $J[\rho]$ being the coulomb energy, $T_s[\rho]$ being the kinetic energy of the non-interacting electrons and $E_{xc}[\rho]$ being the exchange-correlation energy functional. The exchange-correlation functional is expressed as the sum of an exchange functional $E_x[\rho]$ and a correlation functional $E_c[\rho]$, although it contains also a kinetic energy term arising from the kinetic energy difference between the interacting and non-interacting electron systems. The kinetic energy term, being the measure of the freedom, and exchange-correlation energy, describing the change of opposite spin electrons (defining extra freedom to an electron), are the favorable energy contributions. The Coulomb energy term describes the unfavorable electron-electron repulsion energy and therefore disfavors the total electronic energy [35].

In Kohn-Sham density functional theory, a reference system of independent non-interacting electrons in a common, one-body potential V_{KS} yielding the same density as the real fully-interacting system is considered. More specifically, a set of independent reference orbitals ψ_i satisfying the following independent particle Schrödinger equation are imagined:

$$\left[-\frac{1}{2}\nabla^2 + V_{KS}\right]\psi_i = \varepsilon_i\psi_i \tag{3.4}$$

with the one-body potential V_{KS} defined as:

$$V_{KS} = v(r) + \frac{\partial J[\rho]}{\partial \rho(r)} + \frac{\partial E_{xc}[\rho]}{\partial \rho(r)} \tag{3.5}$$

$$V_{KS} = v(r) + \frac{\rho(r')}{|r - r'|} dr' + v_{xc}(r) \tag{3.6}$$

where $v_{xc}(r)$ is the exchange-correlation potential. The independent orbitals ψ_i are known as Kohn-Sham orbitals and give the exact density by:

$$\rho(r) = \sum_{i}^{N} |\psi_i|^2 \tag{3.7}$$

if the exact form of the exchange-correlation functional is known. However, the exact form of this functional is not known and approximate forms are developed starting with the local density approximation (LDA). This approximation gives the energy of a uniform electron gas, i. e. a large number of electrons uniformly spread out in a cube accompanied with a uniform distribution of the positive charge to make the system neutral. The energy expression is:

$$E[\rho] = T_s[\rho] + \int \rho(r) v(r) dr + J[\rho] + E_{xc}[\rho] + E_b \tag{3.8}$$

where E_b is the electrostatic energy of the positive background. Since the positive charge density is the negative of the electron density due to uniform distribution of particles, the energy expression is reduced to:

$$E[\rho] = T_s[\rho] + E_{xc}[\rho] \tag{3.9}$$

$$E[\rho] = T_s[\rho] + E_x[\rho] + E_c[\rho] \tag{3.10}$$

The kinetic energy functional can be written as:

$$T_s[\rho] = C_F \int \rho(r)^{5/3} dr \tag{3.11}$$

where C_F is a constant equal to 2.8712. The exchange functional is given by:

$$E_x[\rho] = -C_x \int \rho(r)^{4/3} dr \tag{3.12}$$

with C_x being a constant equal to 0.7386. The correlation energy, $E_c[\rho]$, for a homogeneous electron gas comes from the parametrization of the results of a set of quantum Monte Carlo calculations.

The LDA method underestimates the exchange energy by about 10 per cent and does not have the correct asymptotic behavior. The exact asymptotic behavior of the exchange energy density of any finite many-electron system is given by

$$\lim_{x\to\infty} U_x^{\sigma} = -\frac{1}{r} \tag{3.13}$$

U_x^{σ} being related to $E_x[\rho]$ by

$$E_x[\rho] = \frac{1}{2}\sum_{\sigma} \int \rho_{\sigma} U_x^{\sigma} dr \tag{3.14}$$

A gradient-corrected functional is proposed by Becke:

$$E_x = E_x^{LDA} - \beta \sum_{\sigma} \int \rho_{\sigma}^{4/3} \frac{x_{\sigma}^2}{1 + 6\beta x_{\sigma} \sinh^{-1} x_{\sigma}} dr \tag{3.15}$$

where σ denotes the electron spin, $x_\sigma = \frac{|\nabla \rho_\sigma|}{\rho_\sigma^{4/3}}$ and β is an empirical constant (β=0.0042). This functional is known as Becke88 (B88) functional [36].

The adiabatic connection formula connects the non-interacting Kohn-Sham reference system (λ=0) to the fully-interacting real system (λ=1) and is given by:

$$E_{xc} = \int_0^1 U_{xc}^{\lambda} d\lambda \tag{3.16}$$

where λ is the interelectronic coupling-strength parameter and U_{xc}^{λ} is the potential energy of exchange-correlation at intermediate coupling strength. The adiabatic connection formula can be approximated by

$$E_{xc} = \frac{1}{2} E_x^{exact} + \frac{1}{2} U_{xc}^{LDA} \tag{3.17}$$

since $U_{xc}^{0} = E_x^{exact}$, the exact exchange energy of the Slater determinant of the Kohn-Sham orbitals, and $U_{xc}^{1} = U_{xc}^{LDA}$ [37].

The closed shell Lee-Yang-Parr (LYP) correlation functional [38] is given by

$$E_c = -a \int \frac{1}{1 + d\rho^{-1/3}} \left\{ \rho + b\rho^{-2/3} \left[C_F \rho^{5/3} - 2t_w + \left(\frac{1}{9} t_w + \frac{1}{18} \nabla^2 \rho\right) \right] e^{-c\rho^{-1/3}} \right\} dr \tag{3.18}$$

where

$$t_w = \frac{1}{8} \frac{|\nabla \rho(r)|^2}{\rho(r)} - \frac{1}{8} \nabla^2 \rho \tag{3.19}$$

and a=0.04918, b=0.132, c=0.2533 and d=0.349.

The mixing of LDA, B88, E_x^{exact} and the gradient-corrected correlation functionals to give the hybrid functionals [39] involves three parameters.

$$E_{xc} = E_{xc}^{LDA} + a_0\left(E_x^{exact} - E_x^{LDA}\right) + a_x \Delta E_x^{B88} + a_c \Delta E_c^{non-local} \tag{3.20}$$

where ΔE_x^{B88} is the Becke's gradient correction to the exchange functional. In the B3LYP functional, the gradient-correction ($\Delta E_c^{non-local}$) to the correlation functional is included in LYP. However, LYP contains also a local correlation term which must be subtracted to yield the correction term only.

$$\Delta E_c^{non-local} = E_c^{LYP} - E_c^{VWN} \tag{3.21}$$

where E_c^{VWN} is the Vosko-Wilk-Nusair correlation functional, a parametrized form of the LDA correlation energy based on Monte Carlo calculations. The empirical coefficients are a_0=0.20, a_x=0.72 and a_c=0.81 [40].

The DFT functional used in the geometry optimizations and frequency calculations is the Becke 3-parameter-Lee-Yang-Parr exchange-correlation functional (B3LYP) as implemented in the Gaussian 03 package. This functional has been successfully applied to the phosphate hydrolysis reactions in both enzymatic and aqueous media.

B3LYP functional is known to underestimate the reaction barriers so that single point calculations are done with MPWB1K [41] hybrid functional that is parametrized for reaction barrier calculations. MPWB1K contains modified Perdew Wang Exchange functional [42] and Becke 95 as correlation functional.

Given any local exchange correlation DFT:

$$E_{\mathrm{XC}} = E_{\mathrm{XC}}^{\mathrm{DFT}} + a_0\left(E_{\mathrm{X}}^{\mathrm{Exact}} - E_{\mathrm{X}}^{\mathrm{DFT}}\right) \tag{3.22}$$

a_0= 0.28 is employed as the best fit value in the Becke95 correlation functional [43].

Due to its high exact exchange content MPWB1K functional is good at estimating reaction barriers. On the other hand, the high exact exchange content delimits the use of MPWB1K functional in the calculation of ground state properties so that B3LYP functional is used in geometry optimizations instead of MPWB1K.

3.2. Basis Set

All the geometry optimizations were carried out using 6-31+G** basis set in conjunction with the B3LYP method in order to obtain reasonable geometries along with a minimum computational cost.

The 6-31+G** basis set describes the core orbitals by a combination of six primitive Gaussian functions and the valence shell is split into two orbitals consisting of three and one primitive Gaussian functions. "+" designates that 6-31G basis set is supplemented by diffuse functions and "**" designates a set of d functions on heavy atoms and a set of p functions on hydrogen atoms.

3.3. Polarizable Continuum Model (PCM)

Solute solvent interactions can have dramatic effects on molecular energies, structures and properties which can be computed effectively using continuum solvation models. In these models, the solvent is represented as a structureless polarizable medium characterized by its dielectric constant Є, disturbed by solute cavities [44].

In basic continuum solvation models; the solute is described at a homogenous quantum mechanical (QM) level and the solute-solvent interactions are limited to those of electrostatic interaction. The model system is a very dilute solution and the solvent is isotropic, at equilibrium at a given temperature and pressure. Beyond these basic properties, as an important concept in all continuum models, the cavity determines solvent excluding and and solvent accesible surfaces thereby dictating the solute solvent interactions (Figure 2.1).

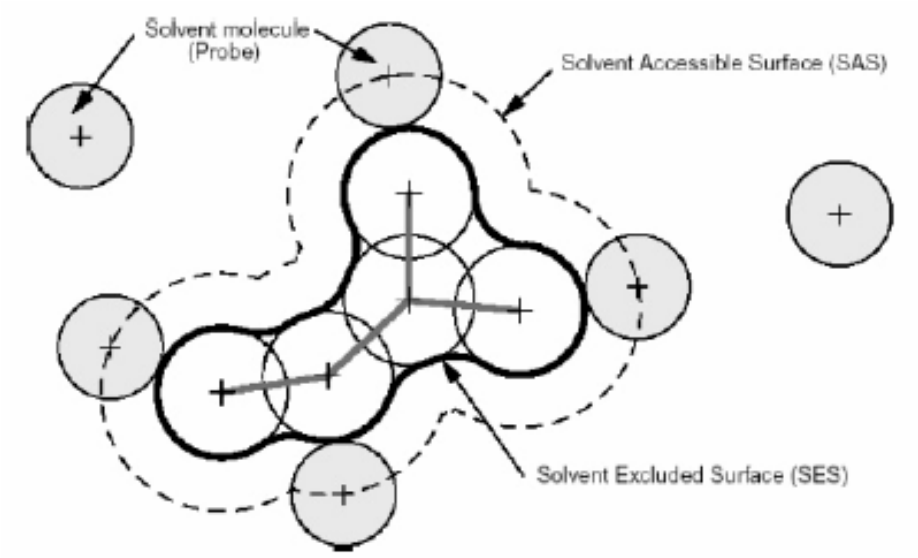

3.1. Solvent exluded surface (SES) and solvent accesible surface (SAS)

The central problem of continuum solvent models is the electrostatic problem described by the general Poisson eqution:

$$-\vec{\nabla}[\epsilon(\vec{r})\nabla\vec{V}(\vec{r})] = 4\pi\rho_{\mathrm{M}}(\vec{r}) \tag{3.23}$$

simplified to:

$$\begin{aligned} -\nabla^2 V(\vec{r}) &= 4\pi\rho_{\mathrm{M}}(\vec{r}) \quad \text{within } C \\ -\epsilon\nabla^2 V(\vec{r}) &= 0 \quad \text{outside } C \end{aligned} \tag{3.24}$$

where C is the portion of space occupied by cavity, Є is dielectric function, V is the sum of electrostatic potential V_M generated by the charge distribution ρ_M and the reaction potential V_R generated by the polarization of the dielectric medium:

$$V(\vec{r}) = V_{\mathrm{M}}(\vec{r}) + V_{\mathrm{R}}(\vec{r}) \tag{3.25}$$

There are many solutions for the electrostatic potential problem involving the electrostatic solute-solvent interaction; such as apparent surface charge (ASC) methods using an axuiliary quantity; an apparent surface charge σ(s) spread on the cavity surface. Among the many solutions to the electrostatic problem is the Integrated Equation Formalism (IEF) as an ASC method originally formulated by Cancẻs and Menucci.

Finally, the solvation free energy, measured with respect to a system composed of the pure unperturbed liquid at equilibrium and by the solute molecules in a seperate phase considered as an ideal gas is given by the following expression [45-47]:

$$\Delta G_{\mathrm{sol}} + \Delta G_{\mathrm{el}} + G_{\mathrm{rep}} + G_{\mathrm{dis}} + G_{\mathrm{cav}} + \Delta G_{\mathrm{tm}} + P\Delta V \qquad (3.26)$$

here "*sol*" denotes solvation, "*el*" denotes electrostatic, "*rep*" denotes repulsion, "*cav*" cavitation.

In this study IEFPCM method implemented in Gaussian 03 program package is used for solvent calculations along with BONDII radii definition for the atoms and dielectric constant of 78.39 for water as solvent. Moreover, standard state corrections are done for explicit water molecules in free energy calculations using C_{water} = 55.6 M .

3.4. Molecular Dynamics (MD)

Molecular dynamics (MD) simulations is one of the principal methods in the theoretical investigation of biological molecules that provides information on the time dependent behaviour of the molecular systems.

Nowadays, molecular dynamics simulations are routinely used to examine the structure, dynamics and thermodynamics of biological molecules and their complexes as well as for the determination of structures form X-ray crystallography and from NMR experiments.

3.4.1. Force Field

At the heart of molecular mechanics lies the force field which describes the potential energy surface of the system. The force field is composed of various contributions like bonded or valence terms (bond stretching, angle bending and torsion angle) and non bonded terms (van der Waals and Coulomb forces) all of which contain emprical parameters fitted to results of experimental studies or high level calculations (Figure 3.2).

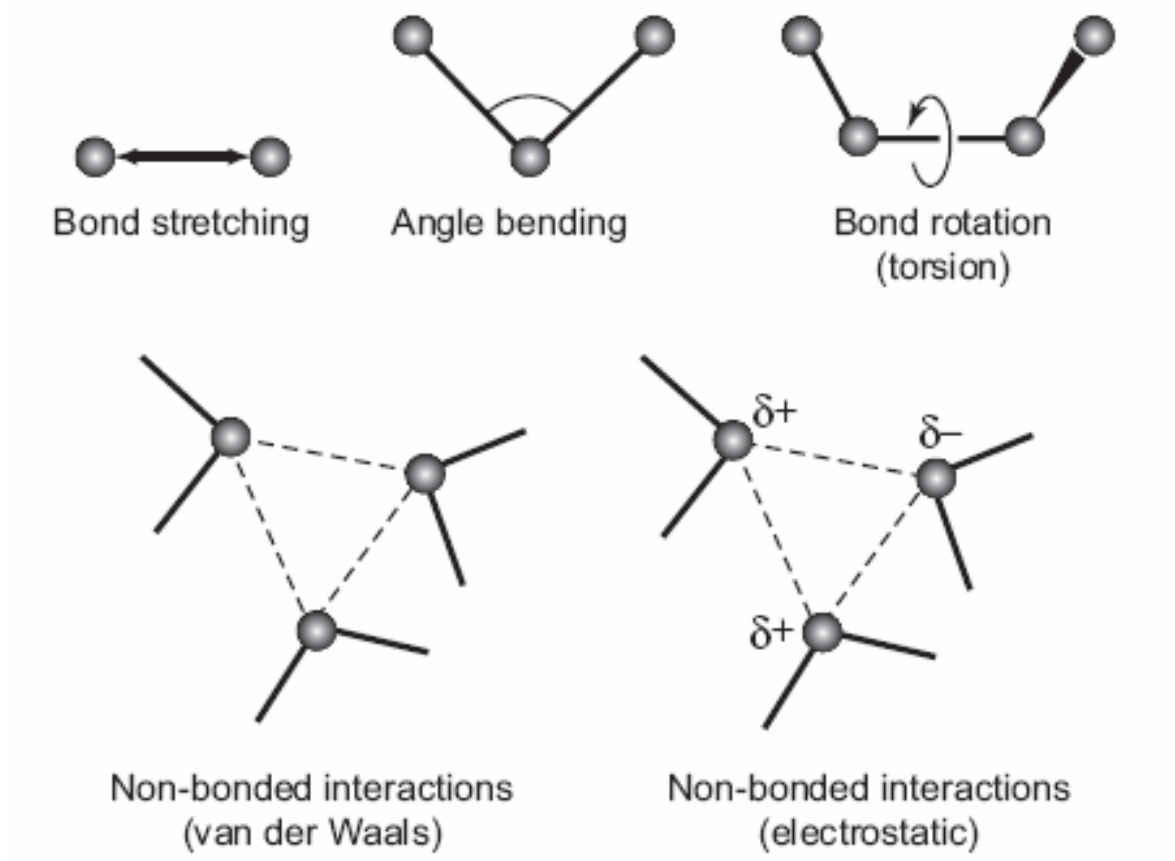

Figure 3.2. Contributions to the force field

In the light of these contributions the potential energy V(R) is defined as:

$$V(\mathbf{R}) = E_{\text{bond}} + E_{\text{angle}} + E_{\text{torsion}} + E_{\text{non-bonded}} \tag{3.27}$$

The specific contibutions to the potential energy can be described as follows:

$$E_{\text{bond}} = \sum_{\text{bonds}} \frac{k_b}{2}(l - l_0)^2 \tag{3.28}$$

where k_b is specific force constant, l is bond length and l_0 is equilibrium bond distance

$$E_{\text{angle}} = \sum_{\text{angles}} \frac{k_\theta}{2}(\theta - \theta_0)^2 \tag{3.29}$$

where k_θ is specific force constant, θ is bond angle and θ_0 is equilibrium bond angle

$$E_{\text{torsion}} = \sum_{\text{torsions}} \frac{V_n}{2}(1 + \cos(n\omega - \gamma)) \tag{3.30}$$

where Vn is the amplitude, n is the number of minima on the potential energy surface, ω is the torsion angle and γ is the phase factor

$$E_{\text{non-bonded}} = \underbrace{\sum_i \sum_{j>i} \left(\frac{A_{ij}}{r_{ij}^{12}} - \frac{B_{ij}}{r_{ij}^{6}} \right)}_{\text{van der Waals}} + \underbrace{\sum_i \sum_{j>i} \frac{q_i q_j}{\varepsilon r_{ij}}}_{\text{Coulomb}} \tag{3.31}$$

where van der Waals interaction between two atoms i and j separated by distance r_{ij} is described by Lenard Jones potential with parameters A_{ij} and B_{ij}, and Coulomb potential is described by electrostatic interaction between a pair of atoms i and j using q_i and q_j as charges on atom and Є as the dielectric constant of medium.

Sometimes force fields contain terms like H–bonding parameters in addition to these basic contibutions as well as variants of these contributions.

3.4.2. Theory of Molecular Dynamics

The state of any classical system can be completely described by means of specifying the positions and momenta of the all particles:

$$\mathbf{q} = (x_1, y_1, z_1, x_2, y_2, z_2, \ldots)$$
$$\mathbf{p} = (p_{x,1}, p_{y,1}, p_{z,1}, p_{x,2}, p_{y,2}, p_{z,2}, \ldots) \tag{3.32}$$

Since a phase point is defined by the positions and momenta of all particles, it determines the location of the next phase point in the absence of outside forces acting upon the system. Therefore, the relationship between two positions in any time interval is given by:

$$q(t_2) = q(t_1) + \int_{t_1}^{t_2} \frac{p(t)}{m} dt \tag{3.33}$$

where;

$$v = \frac{p}{m} \tag{3.34}$$

Similarly, the relationship between any two momentum vectors is:

$$p(t_2) = p(t_1) + m \int_{t_1}^{t_2} a(t) dt \tag{3.35}$$

using Newton's Second Law of Motion:

$$a = \frac{F}{m} \tag{3.36}$$

Moreover, the average value of any property during this time evolution is:

$$\langle A \rangle = \frac{1}{M} \sum_{i}^{M} A(t_i) \tag{3.37}$$

where M is the number of times the property is sampled. In the sampling of continously and following the trajectory indefinitely, this equation becomes [48]:

$$\langle A \rangle = \lim_{t \to \infty} \frac{1}{t} \int_{t_0}^{t_0+t} A(\tau) d\tau \tag{3.38}$$

assuming ergodic hypothesis to be valid and independent of choice of t_0.

3.4.3. Practical Aspects

The coordinates of the X-ray structure of elongation factor Tu of thermus aquaticus in the Brookhaven Protein DataBank (1EFT) [3] is used for the starting conformation of the MD simulation. The force field parameters for GTP molecule is obtained from the literature [49]. All protons are added in their standard geometric positions using the AMBER 8.0 program [50]. The resulting structure is then energy-minimized with SANDER program in a truncated octahedron box containing TIP3P explicit water molecules.

The simulation is performed with the AMBER force field version ff03 under periodic boundary conditions with an integration time step of 2 fs. The SHAKE algorithm is applied to all bond lengths involving a hydrogen atom. A cut-off of 9 Å is used for non-bonded interactions. The initial temperature is set to 10 K and raised to 300 K in about 15 ps. A total of 15 ns simulation is performed with PMEMD (Particle Mesh Ewald Molecular Dynamics) under constant pressure conditions recording the coordinates in every 40 fs.

4. RESULTS AND DISCUSSION

4.1. Phosphate Hydrolysis

Phosphate hydrolysis reactions have been studied from many distinct perspectives in the literature using different computational approaches and different model systems. Namely, gas phase optimizations, gas phase optmizations followed by single point calculations in solvent medium and coupled potential methods (QM/MM) were tried as alternative methods for the investigation of the hydrolysis reaction.

In addition to these, different model systems, like mono phosphates, pyrophosphates, triphosphates and different protonation states of these were employed in the studies. Moreover, Mg^{+2} ion is also included in some studies for the phosphate hydrolysis reaction.

In the results of these studies, different pathways for the phosphate hydrolysis reaction were proposed, presumably stemming from the different computational approaches and model systems employed by the individual studies.

The aim of this study is to elucidate the phosphate hydrolysis mechanism comprehensively using quantum mechanical tools without neglecting any significant contribution to the mechanism of the reaction. For this reason, solvent optimizations along with analytic frequency calculations are done in order to include the solvation effects and estimate free energies of activations ($\Delta G^{\pm}$) for the reactions.

Moreover, the phosphate hydrolysis reaction is investigated in different dielectric environments in the presence or absence of Mg^{+2} ion to evaluate the contribution of these factors to the reaction. Also, the reaction coordinate is monitored in detail in order to examine the contribution of different factors to the $\Delta G^{\pm}$.

4.1.1. Methyl Pyrophosphate Trianion Hydrolysis in the Presence of Mg^{+2}

The hydrolysis of methyl pyrophosphate trianion ($CH_3P_2O_7^{-3}$) in the presence of the Mg^{+2} ion is investigated in order to observe the fundamental features of the associative and dissociative mechanisms as well as to reproduce the available experimental and computational results.

$$CH_3P_2O_7^{-3} + H_2O \longrightarrow H_2PO_4^{-} + CH_3PO_4^{-2} \qquad 4.1$$

The system used for the calculations consists of the methyl pyrophosphate trianion, attacking water molecule, Mg^{+2} ion and four water molecules coordinated to the Mg^{+2} ion (Figure 4.1-2).

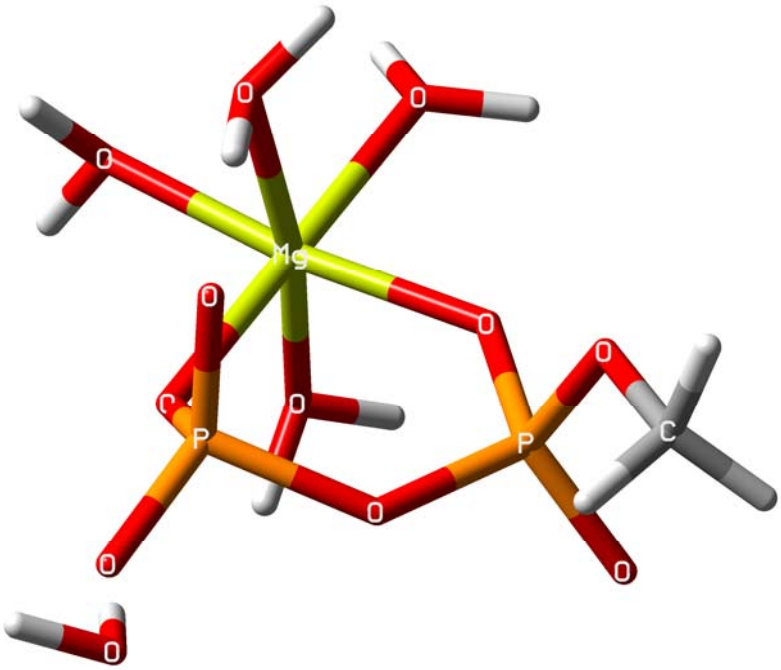

Figure 4.1. R1 (reference reactant) for methyl pyrophosphate Mg^{+2} system

In Figure 4.1 and in the following figures the gray tubes will represent carbon atoms, the white tubes hydrogen atoms, the red tubes oxygen atoms, the orange tubes phosphorus atoms and the green tube the Mg^{+2} ion.

From here on, numbering systems will be used to denote the corresponding atoms in relevant figures along with their atomic symbols.

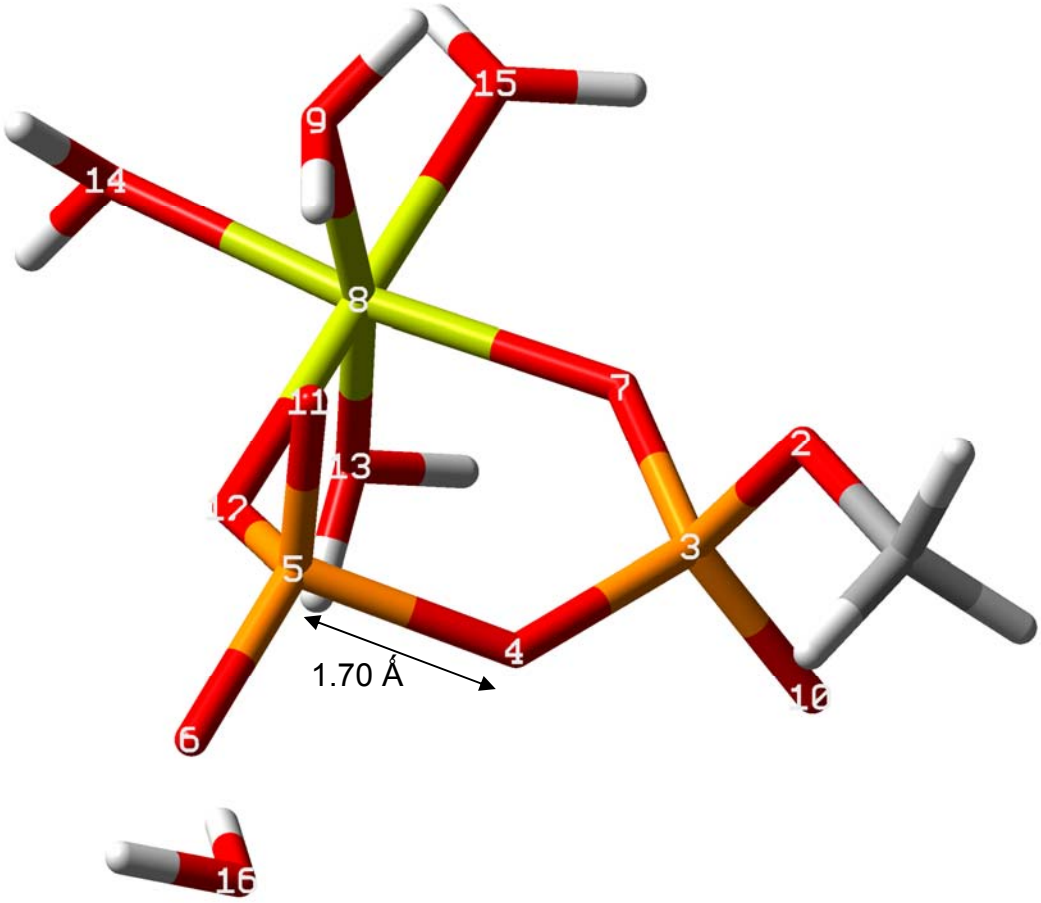

Figure 4.2. Numbering system used for R1

Table 4.1. Wiberg bond orders of R1 (B3LYP/6-311+G(2df,2p))

Wiberg Bond Orders	
P3-O4	0.666
O4-P5	0.549
P5-O16	0.004

Two different transition states are located using this model system. One of these TSs have dissociative character; DTS1 (Figure 4.3) and one of them has an associative character; ATS1 (Figure 4.4) as characterized by the Wiberg bond orders between the oxygen of attacking water molecule (O_W) and phosphorus atom of beta phosphate group (P_β) along with the bond orders between the bridge oxygen atom (O_B) and the phosphorus atom of beta phosphate group (P_β) (Table 4.2-3).

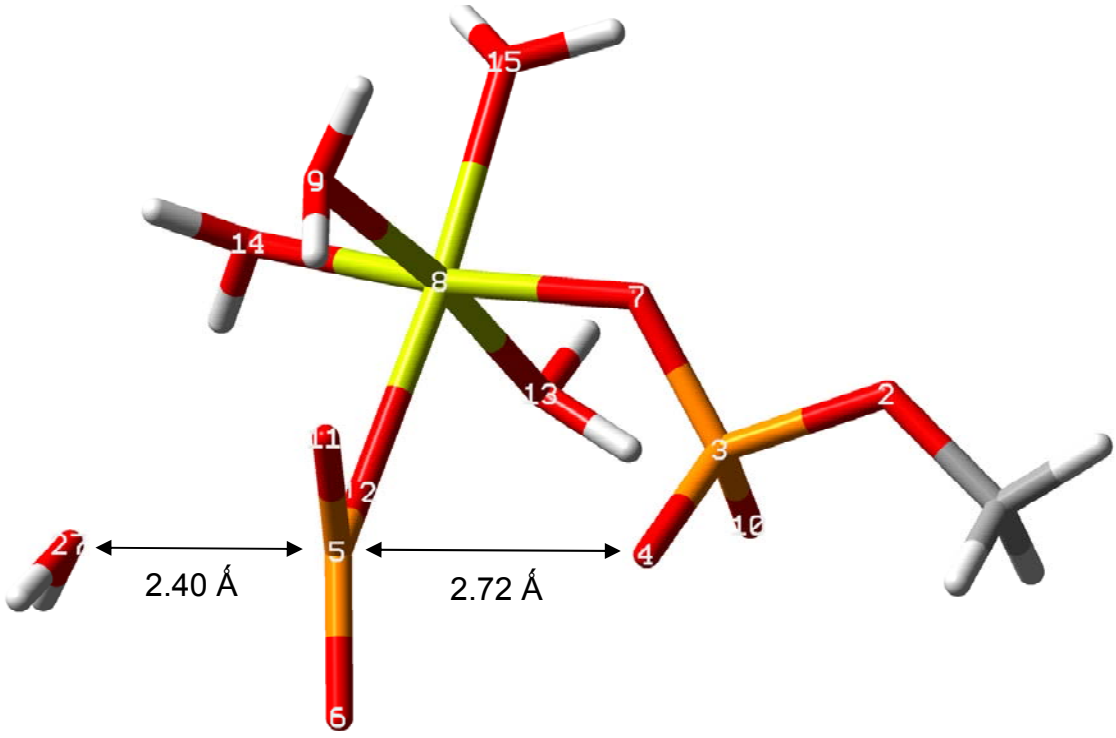

Figure 4.3. Numbering system used for DTS1

Table 4.2. Wiberg bond orders of DTS1 (B3LYP/6-311+G(2df,2p))

Wiberg Bond Orders	
P3-O4	1.006
O4-P5	0.052
P5-O27	0.106

The bond orders are used to analyze the TSs instead of bond lengths in order to present the extent of bond formation or cleavage properly as the sole distances between atoms do not give this specific information clearly.

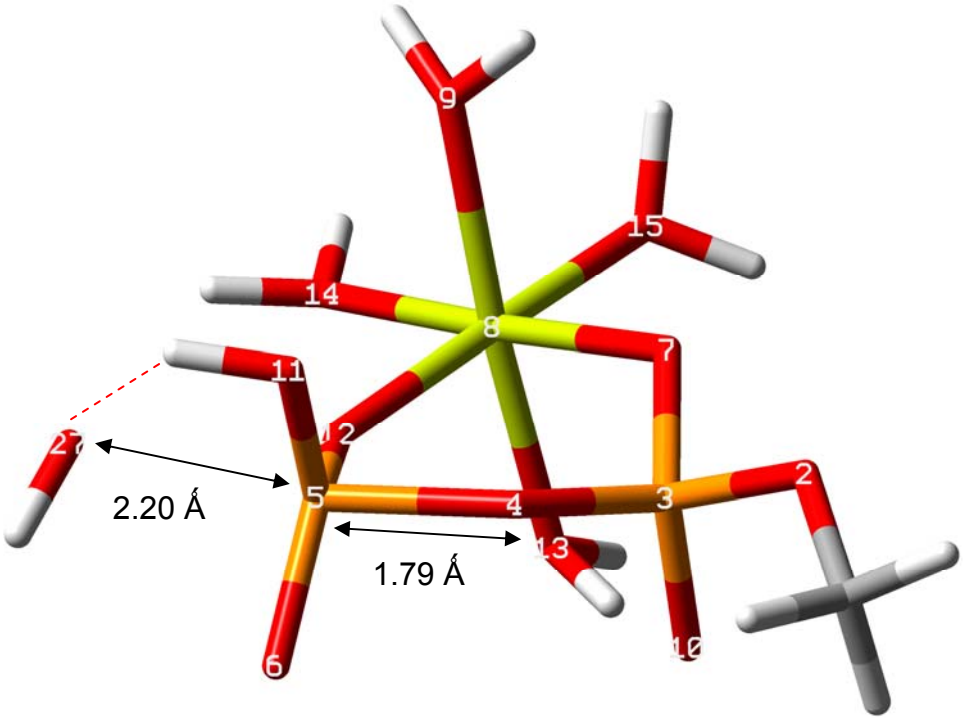

Figure 4.4. Numbering system used for ATS1

Table 4.3. Wiberg bond orders of ATS1 (B3LYP/6-311+G(2df,2p))

Wiberg Bond Orders	
P3-O4	0.746
O4-P5	0.468
P5-O27	0.251

When the Wiberg bond orders of each TS are compared with the bond orders of the R1, two distinct behaviours are observed. In the ATS1 case, a bond is being formed between O_W and P_β without significant cleavage of the bond between P_β (P5) and O_B (O4) displaying a penta coordinated structure which is characteristic for associative TSs.

On the other hand, in the DTS1 case, the bond between P_β and O_B is broken to an important extent without formation of an appreciable bonding interaction between O_W and P_β creating a metaphosphate like structure that is characteristic for dissociative TSs.

Table 4.4. ΔE values of DTS1 and ATS1

ΔE (kcal/mol) Values In Reference To R1			
TS	**B3LYP/6-31+G****	**B3LYP/6-311+G(2df,2p)**	**MPWB1K/6-311+G(2df,2p)**
DTS1	27.2	31.1	33.9
ATS1	39.9	41.2	39.6

In a recent study by Klåhn et. al., it was stated that associative, dissociative and concerted mechanisms are equally probable and separated by only about 1 kcal/mol in the reaction barriers in the Mg^{+2} methyl pyrophosphate trianion system [16].

However, our results (Table 4.4) indicate that the dissociative pathway for the hydrolysis (DTS1) of methyl pyrophosphate trianion is more favourable than the associative pathway (ATS1) with a ΔE difference of about 10 kcal/mol. The principal difference between this study and the former one is that, a transition state structure with a high associative character is located in this one whereas the associative TS in the former one seems to be a dissociative TS rather than an associative one as judged by the bond distances reported in reference 16.

In addition to ΔE values, the ΔG values also confirm that the dissociative path for the hydrolysis of methyl pyrophosphate trianion is more favorable (Table 4.5). The energy difference between the associative pathway (ATS1) and the dissociative pathways (DTS1) increases in ΔG values compared to differences ΔE values.

Table 4.5. ΔG values of DTS1 and ATS1

ΔG (kcal/mol) Values	
TS	**B3LYP/6-31+G****
DTS1	29.8
ATS1	44.8

This increase in energy difference can be explained in terms of entropic contributions as the entropy decreases in the associative path and increases in the dissociative paths during the reaction coordinate. In the associative path, the attacking water molecule and the methyl pyrophosphate trianion combine to form a penta-valent structure decreasing the entropy whereas in the dissociative paths, methyl pyrophosphate trianion is separated into metaphosphate and methyl mono phosphate structures increasing the entropy.

Beyond all these, the available experimental studies report a $\Delta G^{\pm}$ value of 28 kcal/mol [16] for the hydrolysis of methyl pyrophosphate trianion in the presence of the Mg^{+2} ion which is very close to the calculated $\Delta G^{\pm}$ value of 29.8 kcal/mol for the DTS1 structure.

4.1.2. Water Assisted Methyl Pyrophosphate Trianion Hydrolysis

In this part of the study, the hydrolysis of methyl pyrophosphate trianion is investigated using proton relay mechanisms that involve additional water molecules to the attacking water molecule.

This alternative approach to the hydrolysis reaction is based on the idea that additional water molecules can assist the proton transfer from the attacking water molecule to the methyl pyrophosphate trianion while reducing the strain in the transition states by forming six or eight membered TSs rather than four membered ones as in ATS1.

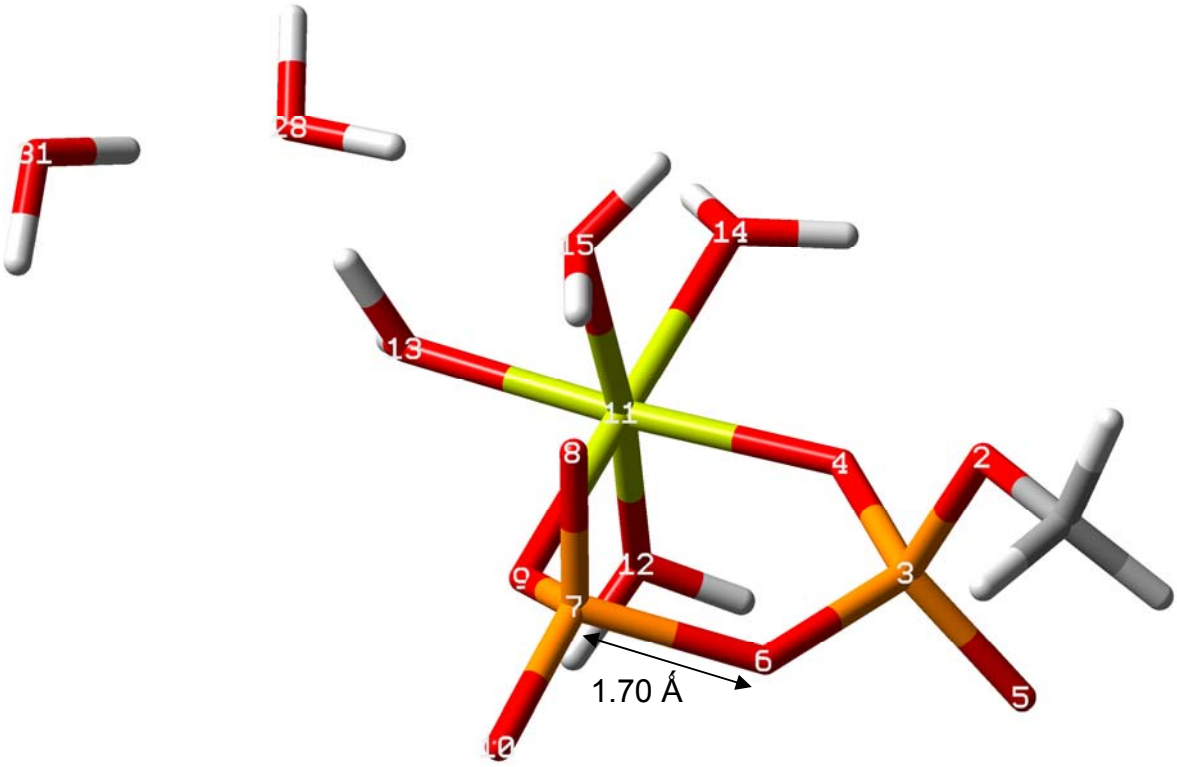

Figure 4.5. Numbering system used for R2

Table 4.6. Wiberg bond orders of R2 (B3LYP/6-311+G(2df,2p))

Wiberg Bond Orders	
P3-O6	0.668
O6-P7	0.547
P7-O31	0.000

The effect of additional water molecules to the reaction mechanism is studied by two different systems; one of which contains one additional water molecule (R2) (Figure 4.5, Table 4.6) whereas the other one contains two additional water molecules (R3) (Figure 4.8, Table 4.11). In the R3 system one of the the additional water molecules is not participating to the reaction and is used only for the ease of optimization.

In the R2 system two different TSs are located; one with an associative character (ATS2) (Figure 4.6.) and the other with a dissociative character (DTS2) (Figure 4.7), again confirmed by the Wiberg bond order calculations (Table 4.7-8). The bond orders data for ATS2 and DTS2 displays general features of associative and dissociative TSs respectively in relation to bond orders of O_W-P_β (O12-P9) and P_β-O_B (P9-O8).

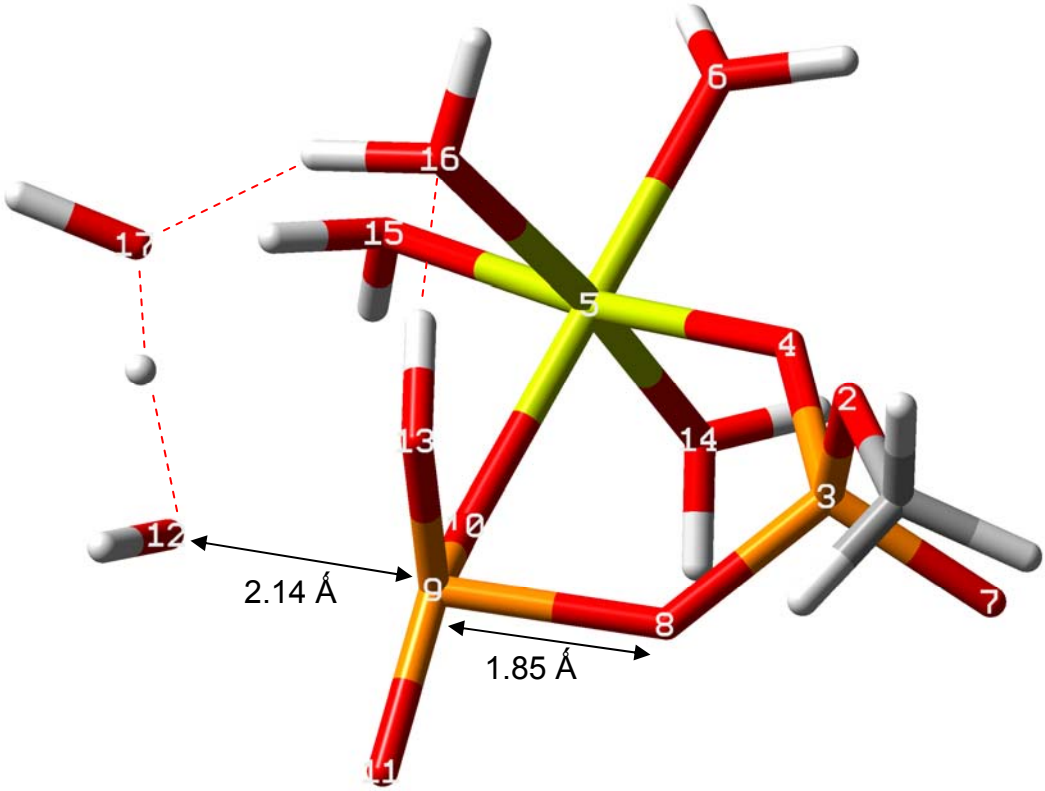

Figure 4.6. Numbering system used for ATS2

Table 4.7. Wiberg bond orders of ATS2 (B3LYP/6-311+G(2df,2p))

Wiberg Bond Orders	
P3-O8	0.770
O8-P9	0.424
P9-O12	0.265

Although both the ATS2 and DTS2 structures display proton relay mechanisms, in ATS2 the proton is transferred to a β oxygen forming an hydroxide ion in place of attacking water molecule whereas in DTS2 the proton is transferred to a α oxygen and hydroxide ion forms in place of the extra water molecule.

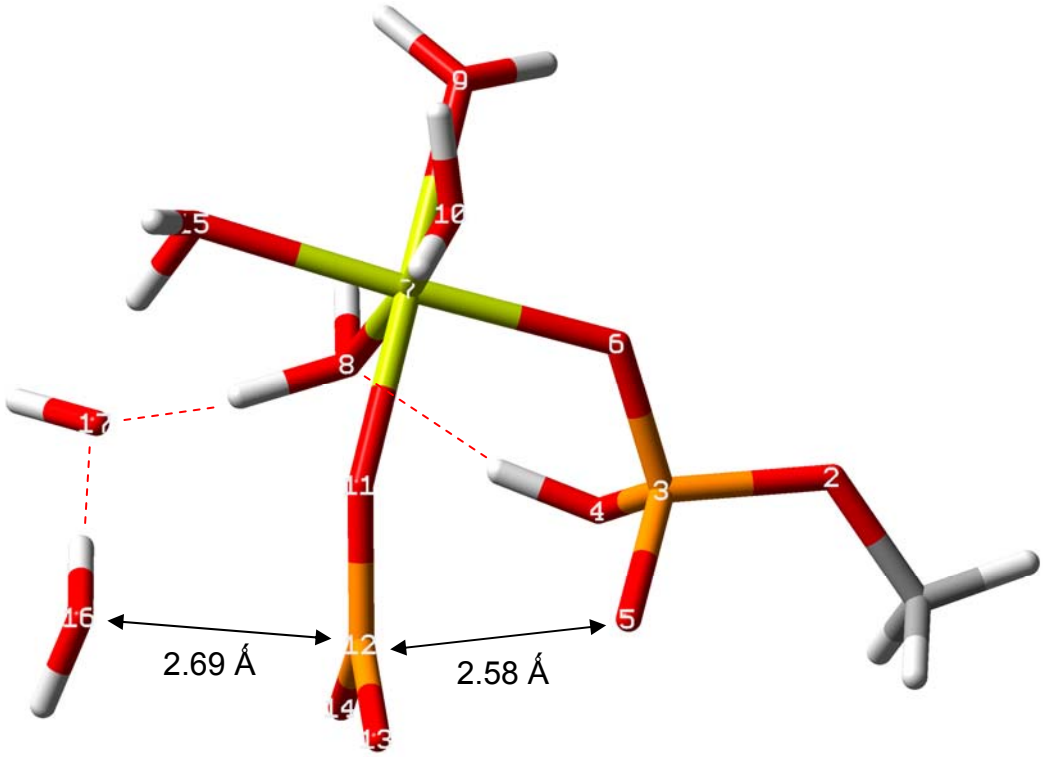

Figure 4.7. Numbering system used for DTS2

Table 4.8. Wiberg bond orders of DTS2 (B3LYP/6-311+G(2df,2p))

Wiberg Bond Orders	
P3-O5	1.062
O5-P12	0.067
P12-O16	0.052

The ΔE values of ATS2 and DTS2 (Table 4.9) indicate that both the associative and dissociative pathways are probable with small preference of assocative pathway over the dissociative pathway when an additional water molecule is present to provide a proton relay mechanism.

Table 4.9. ΔE values of DTS2 and ATS2

ΔE (kcal/mol) Values In Reference To R1			
TS	**B3LYP/6-31+G****	**B3LYP/6-311+G(2df,2p)**	**MPWB1K/6-311+G(2df,2p)**
DTS2	36.6	39.1	36.9
ATS2	35.1	38.4	44.1

On the other hand, the ΔG values of ATS2 and DTS2 suggests that DTS2 is slightly more favorable than ATS2.

Table 4.10. ΔG values of DTS2 and ATS2

ΔG (kcal/mol) Values	
TS	**B3LYP/6-31+G****
DTS2	43.6
ATS2	45.2

This difference in preference with respect to ΔE and ΔG values can again be explained in terms of entropic factors as in the case of ATS1 and DTS1.

In the R3 system (Figure 4.8, Table 4.11) two transition states with associative character are located (ATS3 and ATS4) (Figure 4.9-10, Table 4.12-13). The significant difference between these two associative TSs is the path followed during the proton relay mechanism. It should also be noted that, the ATS4 structure is nearly identical to ATS2 except for one additional water molecule facilitating the optimization procedure.

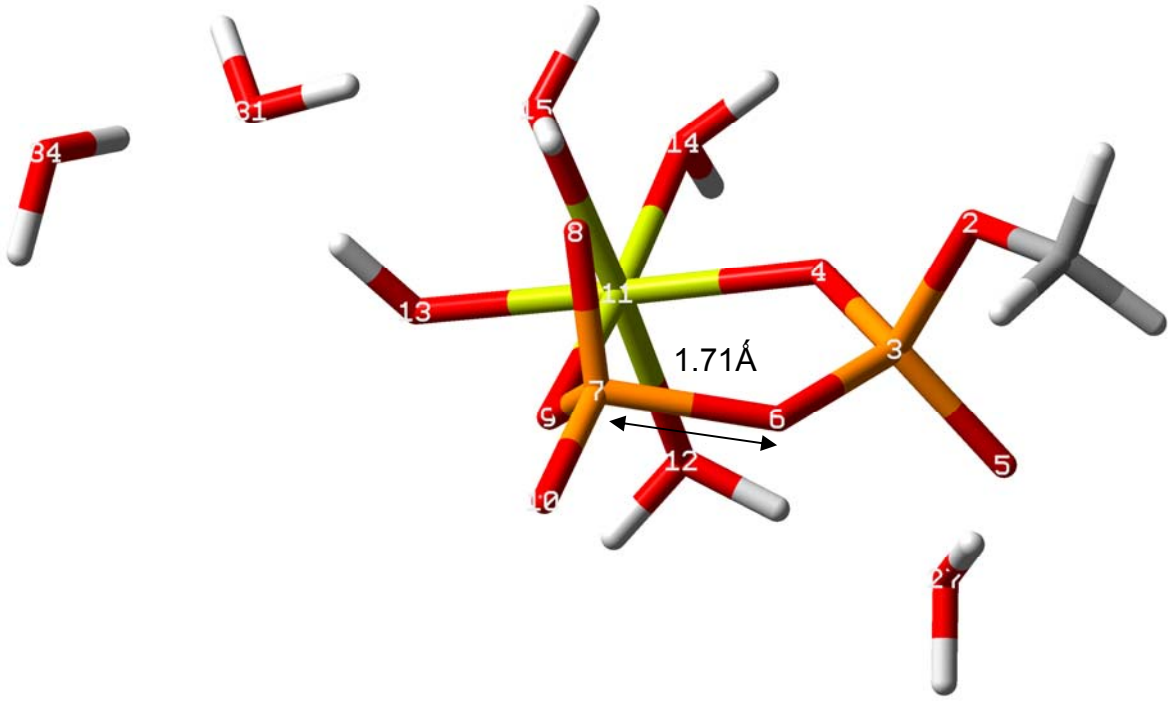

Figure 4.8. Numbering system used for R3

Table 4.11. Wiberg bond orders of R3 (B3LYP/6-311+G(2df,2p))

Wiberg Bond Orders	
P3-O6	0.679
O6-P7	0.535
P7-O34	0.000

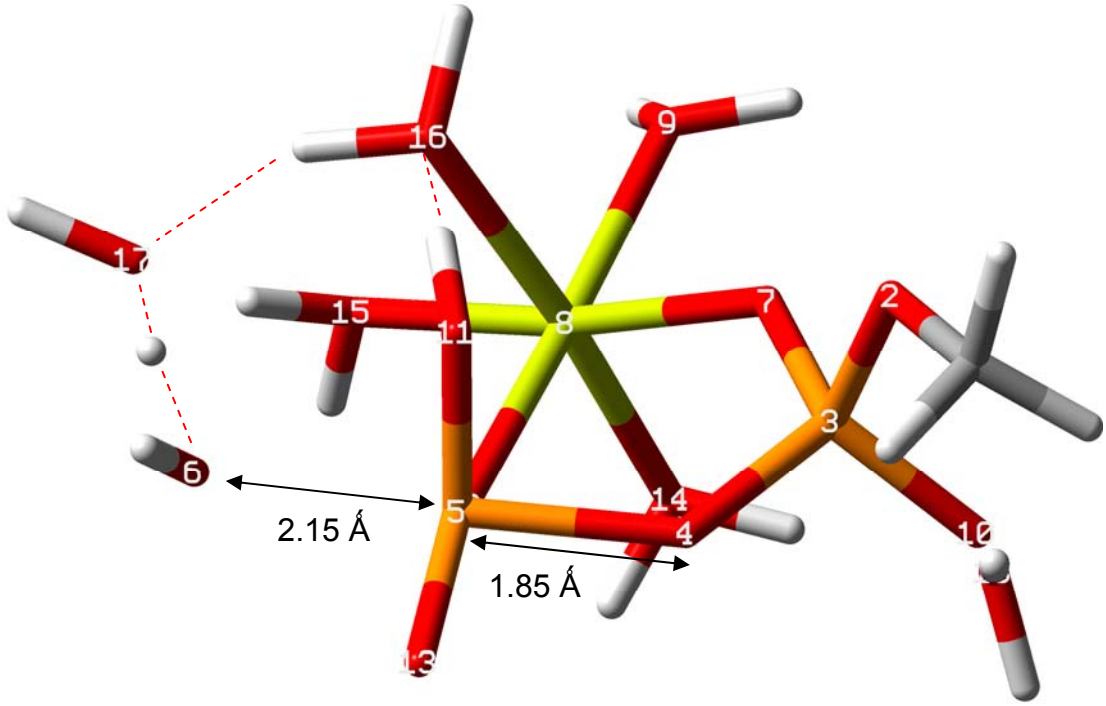

Figure 4.9. Numbering system used for ATS3

Table 4.12. Wiberg bond orders of ATS3 (B3LYP/6-31+G(2df,2p))

Wiberg Bond Orders	
P3-O4	0.7799
O4-P5	0.4183
P5-O6	0.2576

In ATS3, two water molecules, one from the solvent in the near vicinity and one from the Mg^{+2} ion coordination shell assist the proton relay from the attacking water molecule to one of the oxygen atoms of the β phosphate group while the hydroxide ion formed performs a nucleophilic attack to the β phosphate group concertedly. By this way, an eight membered TS is formed instead of a four membered TS like the one in ATS1 (see Figure 4.4)

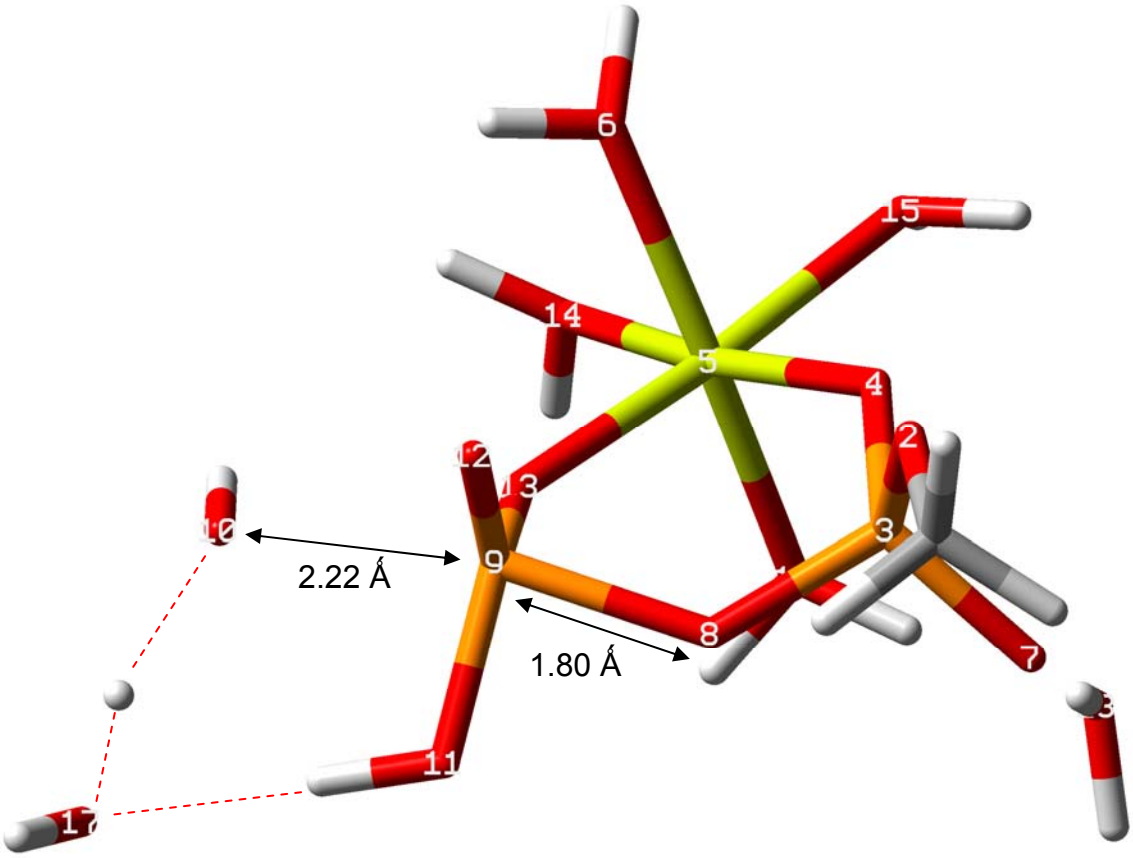

Figure 4.10. Numbering system used for ATS4

Table 4.13. Wiberg bond orders of ATS4 (B3LYP/6-311+G(2df,2p))

Wiberg Bond Orders	
P3-O8	0.7557
O8-P9	0.4578
P9-O10	0.2378

In ATS4, one water molecule from the solvent in the near vicinity assists the proton relay from the attacking water molecule to one of the oxygen atoms of the β phosphate group while the hydroxide ion formed performs a nucleophilic attack to the β phosphate group concertedly. This time a six membered structure (P9-O10-H-O17-H-O11) is formed in the TS.

These two different associative TSs enable us to distinguish between two associative paths; one of which follows a proton relay mechanism over a water molecule coordinated to Mg^{+2} forming an 8 membered TS whereas the other forms a 6 membered TS with the aid of an explicit water molecule. The ΔE values of ATS3 and ATS4 (Table 4.14) suggests that an associative mechanism involving a proton relay mechanism would probably follow a path like the one in ATS3. This could be a result of less strained 8 membered TS structure or proton relay over a water molecule coordinated to the Mg^{+2} ion.

Table 4.14. ΔE values of ATS3 and ATS4

ΔE (kcal/mol) Values In Reference To R3			
TS	**B3LYP/6-31+G****	**B3LYP/6-311+G(2df,2p)**	**MPWB1K/6-311+G(2df,2p)**
ATS3	34.83	37.15	35.59
ATS4	41.17	42.09	40.73

The ΔG values of ATS3 and ATS4 (Table 4.15) also supports the conclusions reached by ΔE values.

Table 4.15. ΔG values of ATS3 and ATS4

ΔG (kcal/mol) Values	
TS	**B3LYP/6-31+G****
ATS3	46.2
ATS4	49.8

The comparison of the ΔE values of ATS1, ATS3 and ATS4 demonstrates that the ATS3, with an 8 membered TS, is the most favorable associative TS. However, the ΔG values indicate that ATS1 is the most favorable route for an associative path. The difference in the ΔE and the ΔG values could be explained by noting the entropic cost of the presence of additional water molecules in ATS3 and ATS4 that leads to higher ΔG values. As a result, ATS1 repreresents the most favorable associative TS (that has at least 10 kcal/mol higher reaction barrier than DTS2) for the hydrolysis of methyl pyrophosphate trianion.

On the other hand, the comparison of the ΔE values of DTS1 and DTS2 demonstrates that the presence of additional water molecules does not decrease but increase the reaction barrier for the hydrolyis of methyl pyrophosphate trianion. The hydrolysis reaction in DTS2 leads to the formation of methyl monophosphate monoanion ($CH_3PO_4H^-$) and HPO_4^{-2} as products whereas the products formed in DTS1 are methyl monophosphate dianion ($CH_3PO_4^{-2}$) and $H_2PO_4^-$. Methyl monophosphate monoanion is a better leaving group than methyl monophosphate dianion and in a dissociative TS, a better leaving group is expected to give a lower reaction barrier. However, because of its low basicity, methyl monophosphate is expected to require too much energy to capture a proton from a water molecule. Presumably, the energy needed for the proton transfer is higher than the one which is gained by having a better leaving group. This makes DTS2 an unfavorable TS with respect to DTS1. The larger difference in ΔG values between DTS1 and DTS2 can again be explained by the entropic cost of the presence of an additional water molecule.

In the light of these results, DTS1 seems to be the most favorable route for the hyrolysis of methyl pyrophosphate trianion in the presence of Mg^{+2} ion in water. However, these results do not rule out the possibility of the existence of the TSs other than DTS1 in the active site of enzymes as the protein environment can vastly change the reaction coordinate by specific interactions.

4.1.3. Unimolecular Dissociation of Methyl Pyrophosphate Trianion

A gas phase scan followed by single point calculations at corresponding dielectric values are performed in order to examine the dielectric effect of the environment on the unimolecular dissociation of methyl pyrophosphate trianion ($CH_3P_2O_7^{-3}$) (Figure 4.11-13). Dielectric values of 4 and 78.4 are chosen as the former value resembles the dielectric of the protein environment whereas the latter is the dielectric value of the water. Only the gas phase and Є=78.4 structures are shown as the geometries of Є=4 (UR2 and UTS2) are very similar to those of Є=78.4 (UR3 and UTS3).

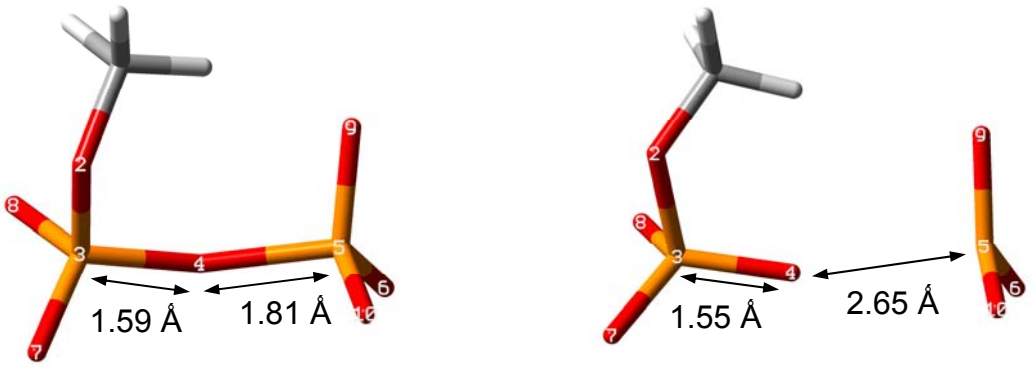

(a) (b)

Figure 4.11. (a) Ground state (UR1) and (b) TS (UTS1) in gas phase

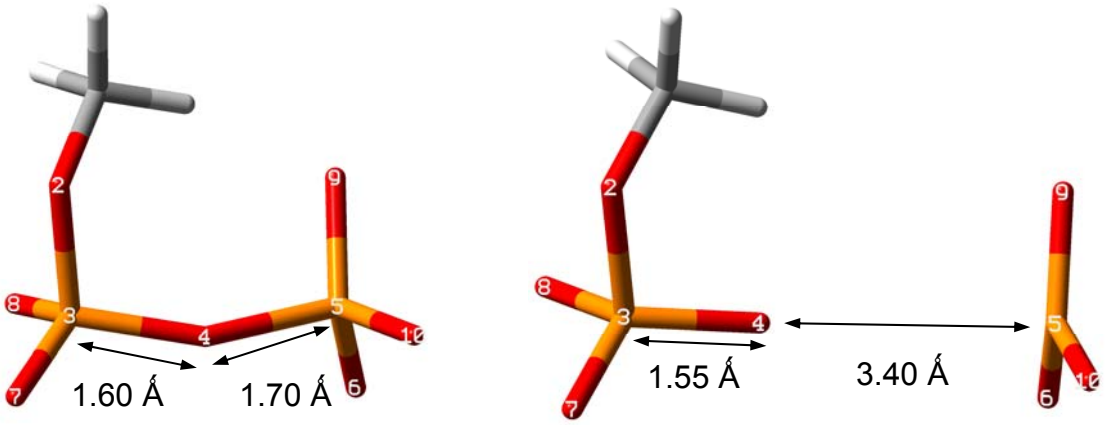

(a) (b)

Figure 4.12. (a) Ground state (UR3) and (b) TS (UTS3) in water

Table 4.16. Wiberg bond orders for UR1, UR2 and UR3 (B3LYP/6-311+G(2df,2p))

Wiberg Bond Orders			
Atoms	**UR1**	**UR2**	**UR3**
P3-O4	0.769	0.705	0.692
O4-P5	0.416	0.493	0.498

Table 4.17. Wiberg bond orders for UTS1, UTS2 and UTS3 (B3LYP/6-311+G(2df,2p))

Wiberg Bond Orders			
Atoms	**UTS1**	**UTS2**	**UTS3**
P3-O4	1.003	1.034	1.028
O4-P5	0.071	0.013	0.006

The plot of distance of $O_B - P_\beta$ versus energy (Figure 4.13) reveals that both the reaction barrier for the unimolecular dissociation of methyl pyrophosphate trianion and the distances between $O_B - P_\beta$ in the TS increase with increasing dielectric of the environment. The solution phase bond cleavage takes place at a much longer $O_B - P_\beta$ distance than in the gas phase. Clearly, the high solution phase barrier originates mainly not from the intrinsic strength of the breaking bond (represented by the gas phase barrier), but from the solvation effects. In other words, the reactant must be better solvated than the transition state because of the differences in their charge distributions.

For the investigation of the charges, Natural Population Analysis (NPA) charges of pyrophosphate oxygen atoms are used as the changes in their charges represents the highest contribution to the differences in the solvation effects that will be examined below.

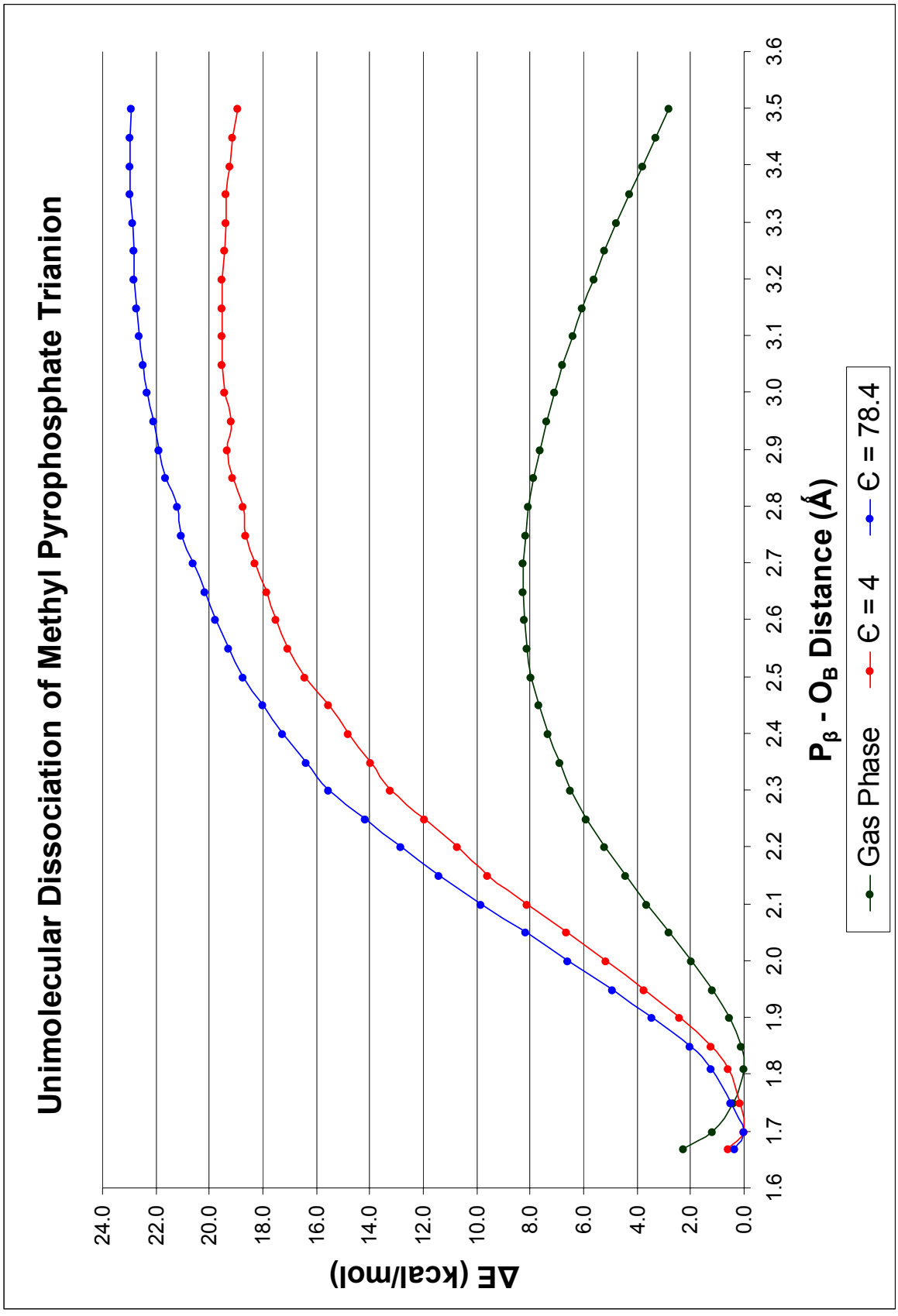

Figure 4.13. Plot of ΔE vs O_B – P_β distance for different dielectric values

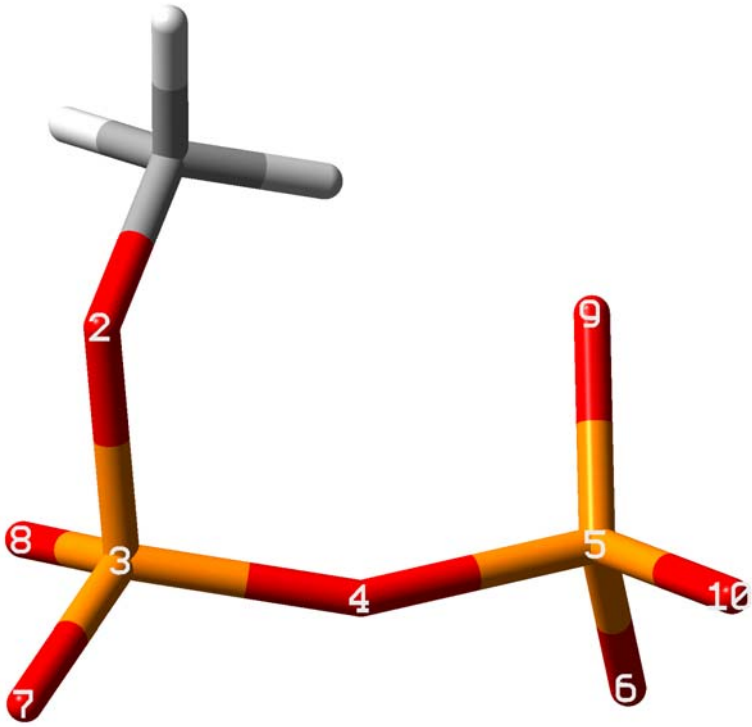

Figure 4.14. Numbering system used for methyl pyrophosphate trianion

Table 4.18. NPA charges of UR1, UR2 and UR3 (B3LYP/6-311+G(2df,2p))

NPA Charges			
Atom	**UR1**	**UR2**	**UR3**
O7	-1.231	-1.242	-1.244
O8	-1.251	-1.238	-1.241
O4	-1.185	-1.180	-1.184
O6	-1.266	-1.286	-1.290
O9	1.274	-1.286	-1.284
O10	-1.258	-1.291	-1.293

Table 4.19. NPA charges of UTS1, UTS2 and UTS3 (B3LYP/6-311+G(2df,2p))

NPA Charges			
Atom	**UTS1**	**UTS2**	**UTS3**
O7	-1.268	-1.283	-1.288
O8	-1.277	-1.295	-1.295
O4	-1.247	-1.264	-1.274
O6	-1.177	-1.157	-1.152
O9	-1.182	-1.157	-1.150
O10	-1.178	-1.157	-1.152

Based on NPA charges, it is clear that the total negative charge on the α non bridging oxygens (O7 and O8) and the β oxygens (O6,O9 and O10) is decreasing, and the negative charge on the bridge oxygen (O4) is increasing while going from ground state to transition state. The total negative charge on the α non bridging oxygens and the β oxygens decreases by 0.2, 0.3 and 0.3 and the negative charge on the bridge oxygen increases by 0.06, 0.08 and 0.09 in gas phase, Є=4 and Є=78.4 respectively.

The solvent can not penetrate close enough to the bridge oxygen so that the bridge oxygen is not well solvated until a certain distance is reached between the $O_B - P_\beta$ (O4-P5). As a result of these, the ground state structures exposing more charge to the solvent are solvated better compared to the transition state structures and the reaction barrier increases with increasing dielectric of the environment (Table 4.20).

Another reason for the increase in reaction barrier may be the screening effect of the solvent molecules represented by the dielectric of the continuum. The repulsion between methyl mono phosphate and metaphosphate arising from negative charges should be higher in the gas phase than the ones in Є=4 and Є=78.4 as these negative charges will be screened to some extent in the latter ones. This stabilizing effect could make the clevage of the bond between $O_B - P_\beta$ more difficult

Table 4.20. ΔE values of UTS1, UTS2 and UTS3

ΔE (kcal/mol) Values			
TS	**B3LYP/6-31+G****	**B3LYP/6-311+G(2df,2p)**	**MPWB1K/6-31+G(2df,2p)**
UTS1	8.4	8.8	14.8
UTS2	21.2	22.3	32.2
UTS3	24.7	25.8	35.7

4.1.4. Unimolecular Dissociation of MPP Trianion in the Presence of Mg^{+2}

The unimolecular dissociation of methyl pyrophosphate trianion ($CH_3P_2O_7^{-3}$) is further investigated in the presence of Mg^{+2} ion in order to analyze the effect the of it on the reaction coordinate and the reaction barrier. This time individual geometries are optimized at Є=78.4 and only a scan at Є=78.4 is performed as our primary aim is to comprehend the hydrolysis of methyl pyrophosphate trianion in aqueous media.

The results of these calculations imply two significant points. The first one is that the presence of Mg^{+2} ion increases the reaction barrier for the unimolecular dissociation of pyrophosphate trianion by its electrostatic interaction between one of the oxygen atoms from the α and β phosphate groups (Figure 4.15).

Secondly, the presence of Mg^{+2} ion changes the charge distribution of methyl pyrophosphate trianion on both ground state and transition state (Figure 4.16-17, Table 4.21-22). As a dication, Mg^{+2} ion effectively reduces the total charge of the system while decreasing the repulsive forces between α and β phosphate groups.

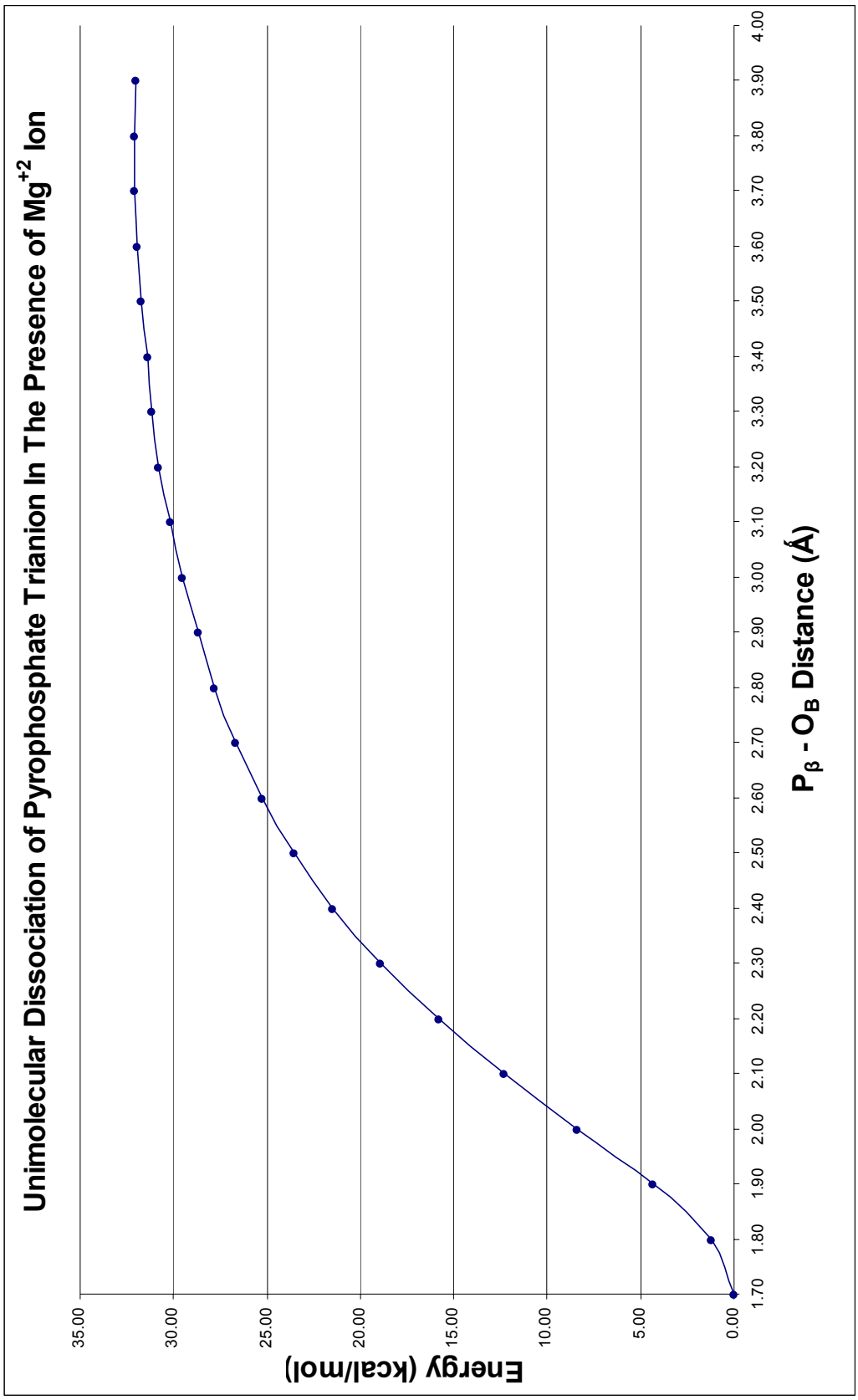

Figure 4.15. Plot of ΔE vs $O_B - P_\beta$ distance

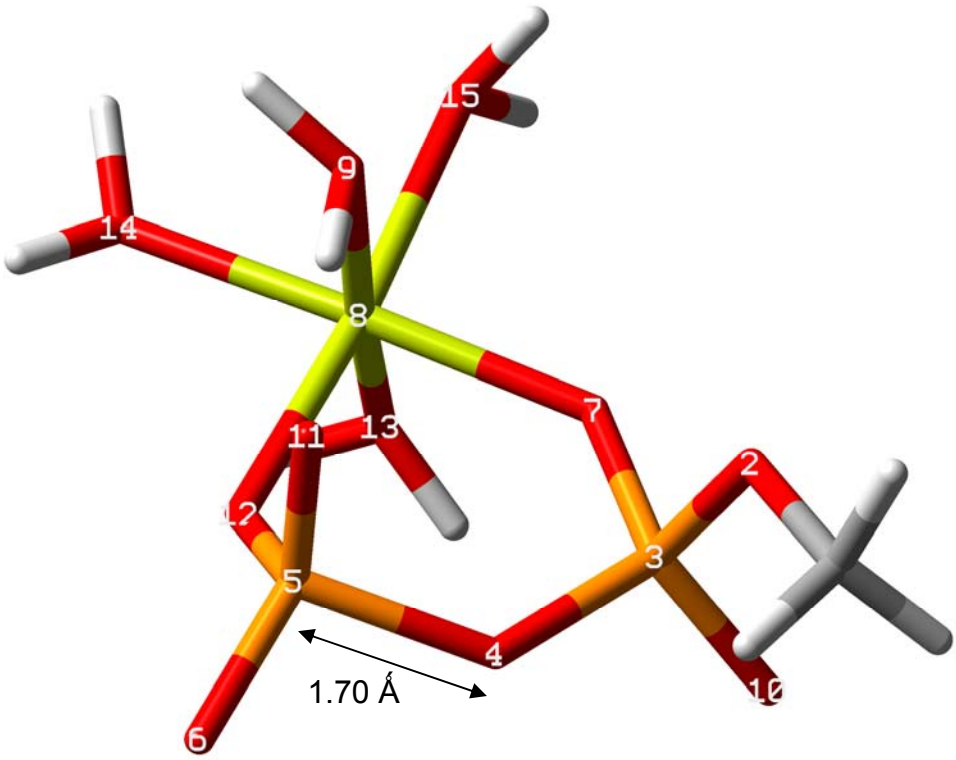

Figure 4.16. Numbering system used for ground state (UR4)

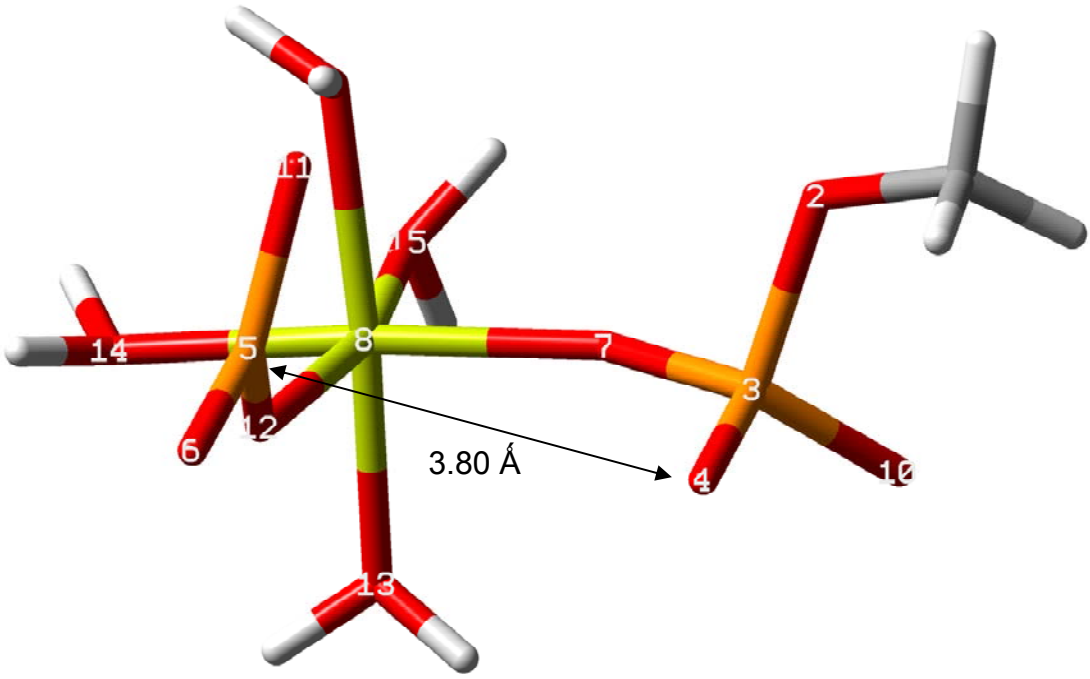

Figure 4.17. Numbering system used for transition state (UTS4)

Table 4.21. Wiberg bond orders for UR4 and UTS4 (B3LYP/6-311+G(2df,2p))

Wiberg Bond Orders		
Atoms	**UR4**	**UTS4**
P3-O4	0.671	1.020
O4-P5	0.539	0.004

Table 4.22. NPA charges for UR4 and UTS4 (B3LYP/6-311+G(2df,2p))

NPA Charges		
Atom	**UR4**	**UTS4**
O7	-1.286	-1.342
O4	-1.157	-1.285
O10	-1.224	-1.301
O6	-1.259	-1.119
O11	-1.257	-1.142
O12	-1.324	-1.201

Table 4.23. ΔE values of UTS4

ΔE (kcal/mol) Values			
TS	**B3LYP/6-31+G****	**B3LYP/6-311+G(2df,2p)**	**MPWB1K/6-31+G(2df,2p)**
UTS4	34.6	35.4	46.4

The ΔE values of UTS4 show that the presence of Mg^{+2} ion increases the reaction barrier by about 10 kcal/mol for the unimolecular dissociation of pyrophosphate trianion compared to the reaction barrier in the absence of Mg^{+2} ion.

The NPA charges indicate that the oxygen atoms coordinated to Mg^{+2} ion have higher total negative charge in the ground state in comparison to transition state so that the Mg^{+2} will be interacting with higher negative charge in the ground state thereby stabilizing the ground state relatively better than the transition state.

The NPA charges also indicate that the decrease of total negative charge on the α non bridging oxygens and the β oxygens is a bit less in the presence of Mg^{+2} ion compared to the pyrophosphate trianion alone with a decrease of 0.25 while the increase of negative charge O_B is higher with a value of 0.13. This larger negative charge accumulation on O_B will increase the solvation energy difference between the ground state and transition state resulting in an increase in the reaction barrier. Moreover, the presence of Mg^{+2} ion decreases the repulsion between α phosphate and β phosphate groups that could also be a factor in the increase of the reaction barrier.

These effects altogether can explain the increase of the reaction barrier for unimolecular dissociation of pyrophosphate in the presence of Mg^{+2}.

4.1.5. Nucleophilic Participation in the Hydrolysis of MPP Trianion

The hydrolysis of methyl pyrophosphate trianion involves a nucleophilic attack from the attacking water molecule to the phosphorus atom of the β phosphate group. In this part, the physicochemisty of this nucleophilic attack is investigated in the presence and absence of the Mg^{+2} ion in order to determine the effects of the Mg^{+2} ion on the nature of the interactions between the attacking water molecule and the β phosphate group.

Two opposing interactions; electrostatic and charge transfer interactions control the nucleophilic attack of the attacking water molecule to the phosphorus atom of the β phosphate group.

Electrostatic interactions consist of the repulsive forces between the negatively charged β phosphate group and the attacking water molecule whereas the charge transfer interactions are attractive, involving significant amount of charge transfer from the attacking water molecule to the phosphate group.

In order to analyze these two interactions, single point calculations are performed by using the DTS1 geometry, as it represents the most favorable path in the hydrolysis of methyl pyrophosphate trianion. First, the Mg^{+2} ion and the water molecules in the coordination shell are omitted and calculations are performed for separate constituents and for complex (Figure 4.18).

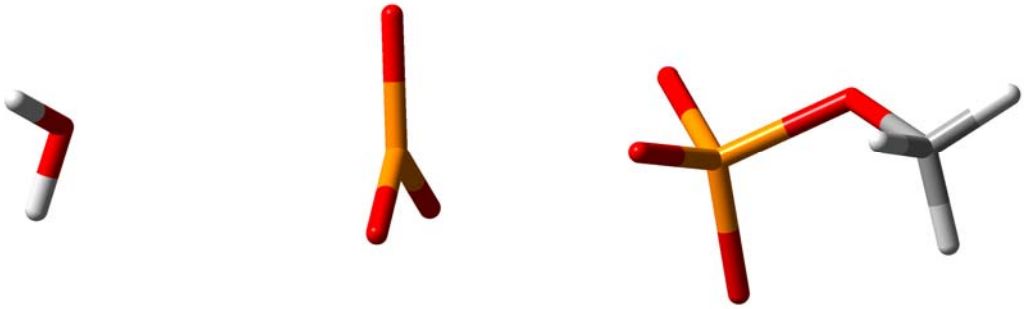

(a) (b)

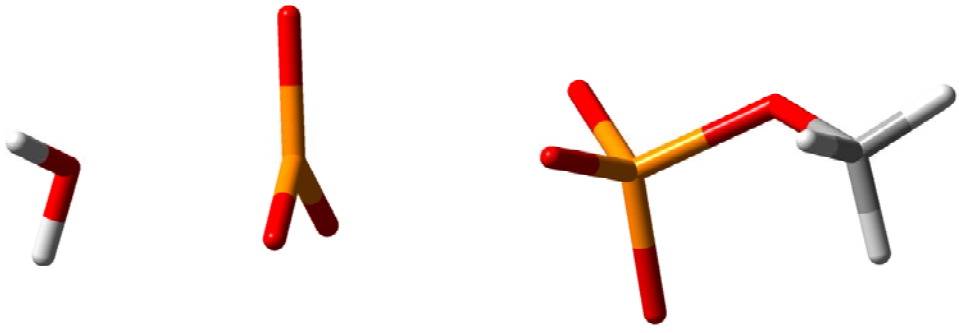

(c)

Figure 4.18. Separated (a) water, (b) MPP, and their complex (c)

The calculations yielded a complexation energy of -0.8 kcal/mol in the absence of the Mg^{+2} ion along with a charge transfer interaction energy of -35.7 kcal/mol. The electrostatic interaction energy is calculated to be 34.9 kcal/mol from the difference of the complexation energy and the charge transfer interaction energy. After this, the same type of calculations are repeated in the presence of the Mg^{+2} ion (Figure 4.19)

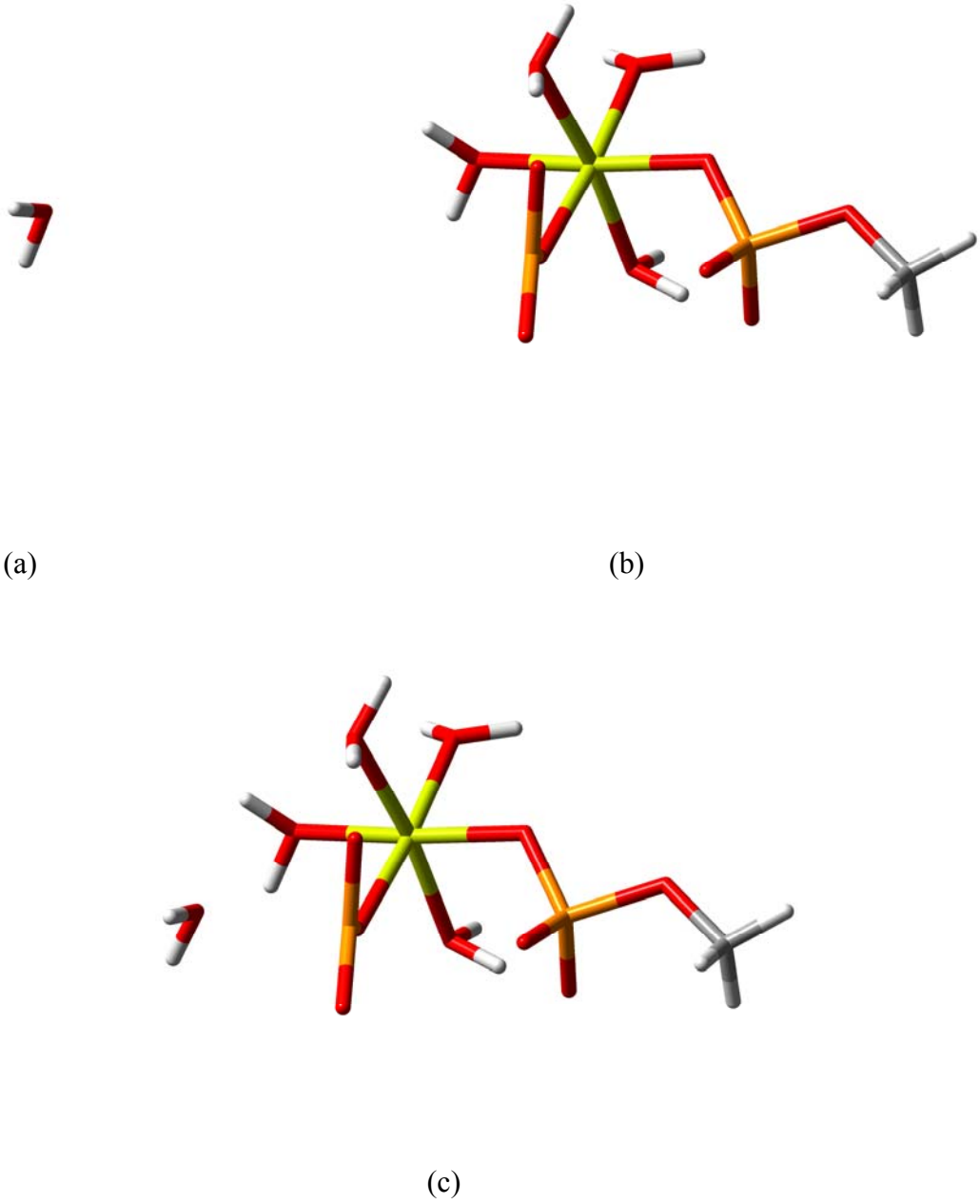

(a) (b)

(c)

Figure 4.19. Separated (a) water, (b) MPP:$Mg^{+2}(OH_2)_4$, and their complex (c)

The calculations yielded a complexation energy of -2.7 kcal/mol in the presence of the Mg^{+2} ion along with a charge transfer interaction enegy of -38.3 kcal/mol. The electrostatic interaction energy is calculated to be 35.6 kcal/mol from the difference of the complexation energy and the charge transfer interaction energy.

These results imply that the presence of the Mg^{+2} ion increases the charge transfer interactions between the attacking water molecule and the β phosphate group of methyl pyrophosphate trianion. The increase in the charge transfer interaction can be explained by the fact that the presence of the Mg^{+2} ion increases the positive charge on the phoshorus atom of the β phosphate group, making it more vulnerable to a nuclophilic attack, and thereby favoring the charge transfer interaction between the attacking water molecule and the β phosphate group.

Taking all these informations into account, a generalization can be made on the nature of the phosphate hydrolysis reactions. If the charge transfer interaction energy is higher than the electrostatic interaction energy, then the phosphate hydrolysis reaction proceeds via a nucleophilic participation. On the other hand, if the electrostatic interaction energy is higher than the charge transfer interaction energy, then phosphate hydrolysis reaction favors a unimolecular dissociation pathway instead of nucleophilic participation.

Moreover, the presence of the Mg^{+2} ion increases the charge transfer interaction energy and therefore favors a nucleophilic participation path for the phosphate hydrolysis reactions. In the methyl pyrophosphate trianion case, it is obvious that in the presence of the Mg^{+2} ion nucleophilic participation (DTS1 with a ΔE value of 27.2 kcal/mol) is more favorable than unimolecular dissociation (UTS4 with a ΔE value of 34.6 kcal/mol).

In order to test the reaction preference in the absence of the Mg^{+2} ion, the transition state structure for the unimolecular dissociation of methyl pyrophosphate trianion in water is located (Figure 4.20) and compared with hydrolysis of methyl pyrophosphate trianion with nucleophilic participation from the literature (Figure 4.21) [16].

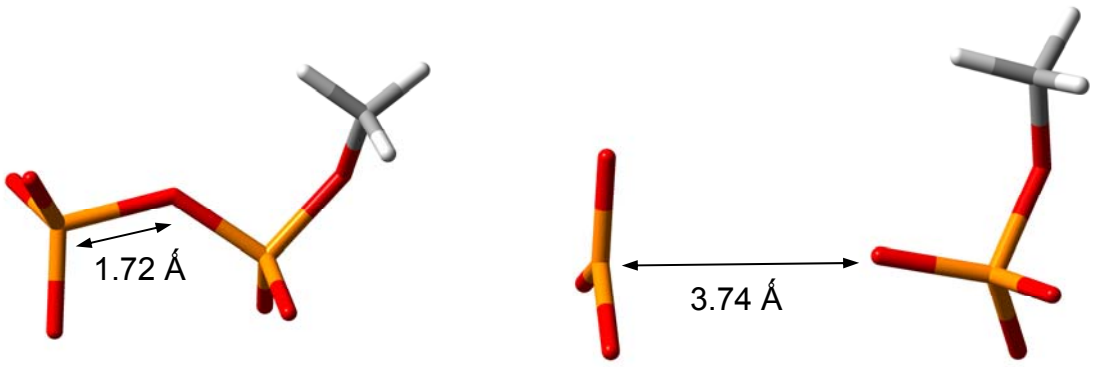

(a) (b)

Figure 4.20. Ground state (a) and transition state (b) for unimolecular dissociation

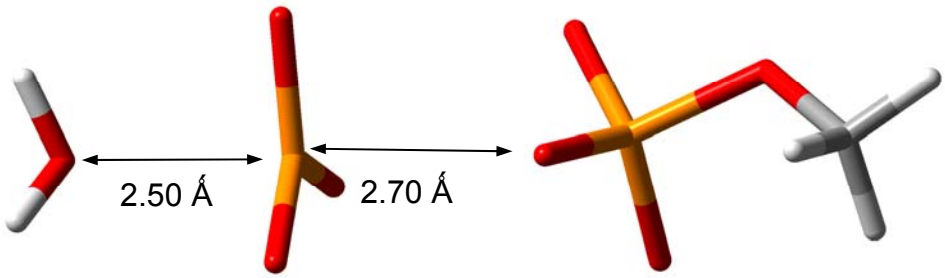

Figure 4.21. Transition state with nucleophilic participation

The results indicate that a TS with unimolecular dissociation (ΔE of 24.0 kcal/mol) is favored over a TS with nuclephilic participation (ΔE of 34.0 kcal/mol) in the absence of the Mg^{+2} ion. The electrostatic interaction energy should be higher in this case compared to the charge transfer interaction energy so that a TS with unimolecular dissociation proceeds with a lower energy barrier than a TS with nucleophilic participation.

In summary, it can be concluded that, in the presence of the Mg^{+2} ion the charge transfer interaction energy is the dominant figure and nucleophilic participation is involved in the TS for the hydrolysis reaction. On the other hand, in the absence of the Mg^{+2} ion the electrostatic interaction energy is the dominant figure and TS for the hydrolysis reaction proceeds via a unimolecular dissociation.

4.1.6. Reaction Coordinate of the Hydrolysis of MPP Trianion

During the hydrolysis reaction the attacking water molecule performs a nucleophilic attack to the terminal phosphate group. However, due to the negative charge of the phosphate group, the attacking water molecule positions itself in a way to reduce the charge dipole interaction between them in the reactant complex. As a result of this positioning, the lone pair electrons of the oxygen atom of the attacking water molecule stands away from the phosphorus atom thereby creating a structure unfavorable for the nucleophilic attack. The attacking water molecule, either in solvent medium or in the active site of EF-Tu, is generally in an unfavourable position for the attack. (Figure 4.22).

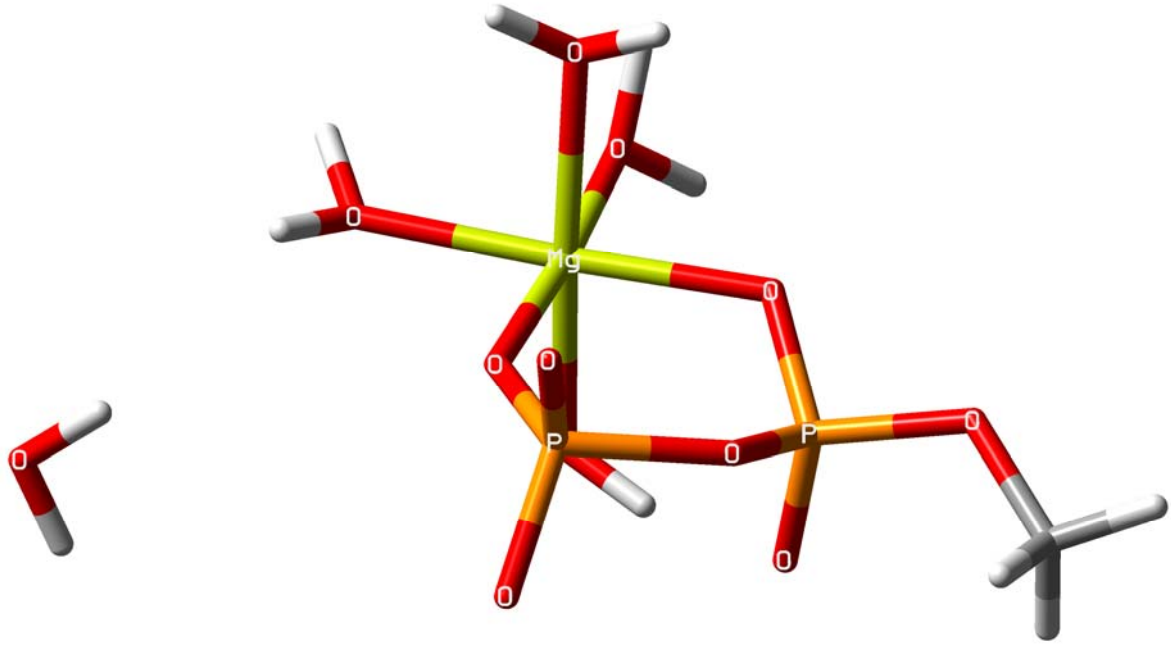

Figure 4.22. Attacking water in unfavourable position

In order to quantify the energy cost for the correct positioning of the attacking water molecule for the nucleophilic attack, two independent calculations are done. The first one involves quantum mechanical calculations in solvent medium whereas the second one involves statistical interpretation of the results of the molecular dynamics simulation of GTP molecule.

4.1.6.1. Quantum Mechanical Interpretation of Reaction Coordinate

In the first one, the reaction coordinate for the hydrolysis reaction of pyrophosphate trianion is examined by performing a potential energy scan on the $O_W - P_\beta$ distance using the R1 system (Figure 4.2) as reference, recording the changes in the bond order (Figure 4.23, Table 4.24).

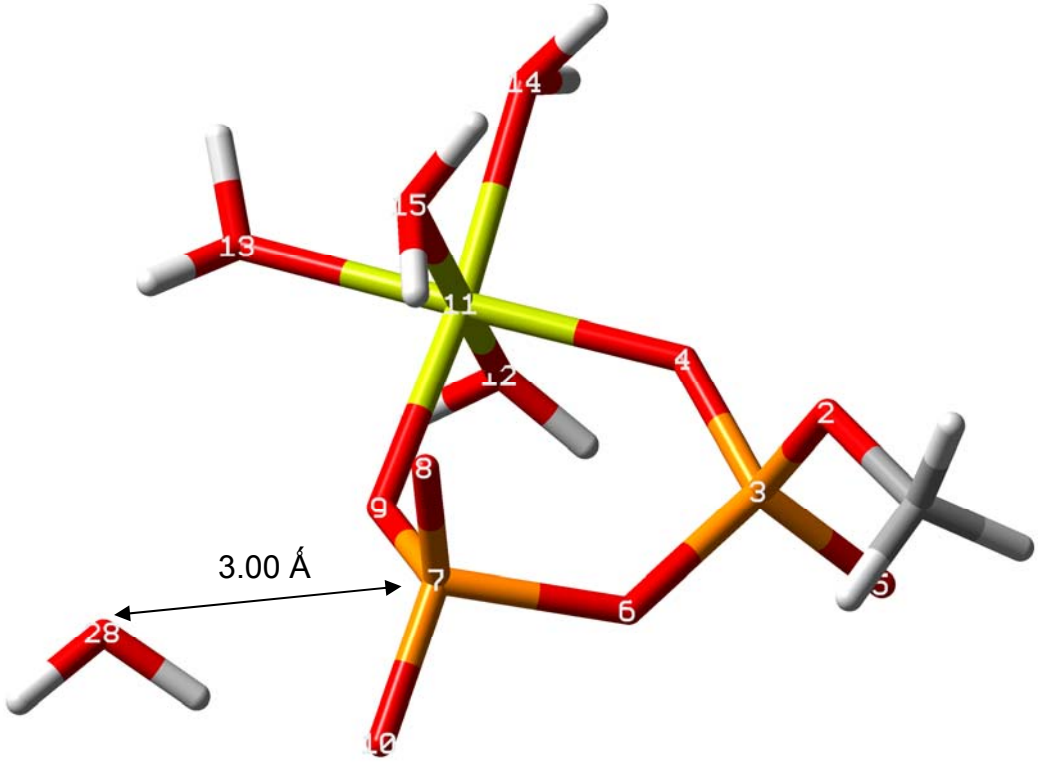

Figure 4.23. Attacking water in favourable position

Table 4.24. Wiberg bond orders for the $P_\beta - O_W$ scan (B3LYP/6-311+G(2df,2p))

Wiberg Bond Orders					
$P_\beta - O_W$ (Å)	2.7	2.8	2.9	3.0	R1
$O_B - P_\beta$	0.518	0.529	0.536	0.540	0.549
$P_\beta - O_W$	0.018	0.010	0.008	0.006	0.004

Table 4.25. ΔE values for the $P_\beta - O_W$ scan

ΔE (kcal/mol) Values		
$P_\beta - O_W$ (Å)	**B3LYP/6-31+G****	**B3LYP/6-311+G(2df,2p)**
2.7	14.1	12.7
2.8	11.5	10.0
2.9	9.0	7.4
3.0	7.2	5.7

The Wiberg bond orders indicate that the bond formation between the oxygen atom (O_W) of the properly positioned water molecule and the phosphorus atom (P_β) of the β phosphate group begins as soon as the distance between them gets shorter than 3.0 Å. In the light of this information, the reaction coordinate of the methyl pyrophosphate trianion hydrolysis, can be divided into two parts; the physical part that describes the correct positioning of the attacking water molecule without bond formation between $O_W - P_\beta$ and the chemical part that describes the bond formation between $O_W - P_\beta$ along with the bond cleavage between $P_\beta - O_B$.

The ΔE values implies that the cost of correct positioning of the attacking water molecule (physical part) amounts to nearly 6 kcal/mol.

4.1.6.2. Molecular Dynamics Simulation of GTP

10 ns of MD simulation of GTP molecule in water clusters is performed in order to observe the positions of water molecules around the GTP molecule. The whole trajectory is screened for possible reactive conformations by searching for geometries that possess certain distance ($O_W - P_\beta < 3.0$ Å) and angle ($170 < H_W - O_W - P_\beta < 180$) constraints. Only 1 out of 22500 geometries have the proper distance and angle values describing a reactive conformation containing a water molecule with a position favoring a nucleophilic attack to the γ phoshate group of GTP (Figure 4.24).

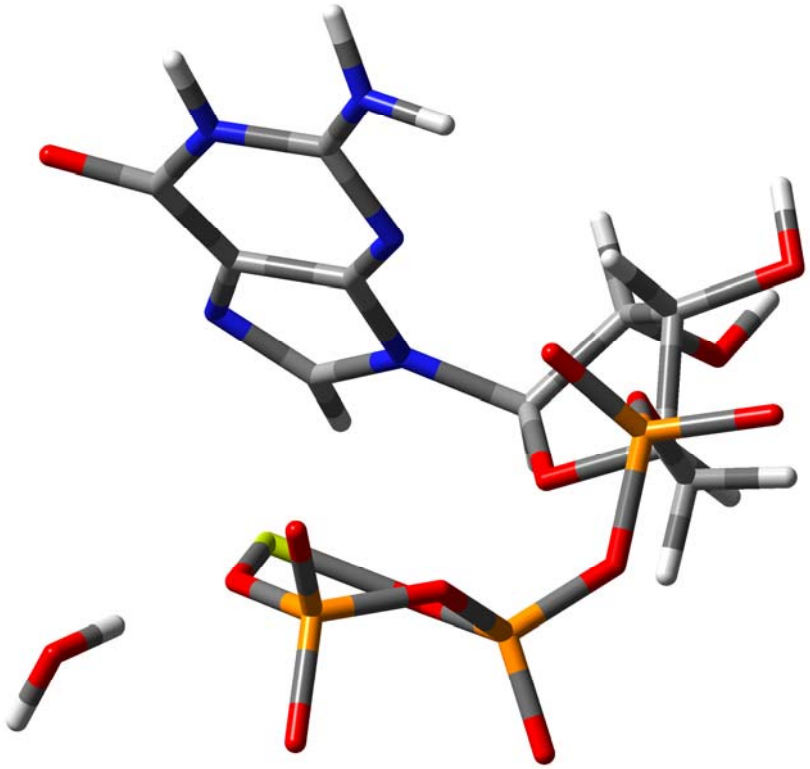

Figure 4.24. H_2O molecule in favourable position for attack

Using simple Boltzmann distribution it can be shown that a ratio of 1/22500 corresponds to 6 kcal/mol energy difference indicating that the energy required to align the attacking H_2O molecule in favorable position is 6 kcal/mol in comparison to average of the ensemble where the lone pair electrons of oxygen atom in the H_2O molecule stands away from the phosphorus atom of the γ phosphate group of GTP.

Quantum and classical mechanical approaches both yield the same result of 6 kcal/mol for the energy cost of the proper alignment of the attacking water molecule for the nucleophilic attack to the phosphate group. 6 kcal/mol energy difference corresponds to approximately four orders of magnitude (10^4) difference in the reaction rates. Based on this observation, it could be suggested that a part of the catalytic contribution of GTPases could be the correct positioning of the attacking water molecule.

In the EF-Tu case, the ribosome induced GTP hydrolysis is 10^5 times faster than the intrinsic GTPase activity and the significant amount of this catalytic effect can be explained by the correct positioning of the attacking water molecule by H85 residue.

4.2. Molecular Dynamics Simulations

In this part of the study, the results of two interrelated molecular dynamics simulations are presented; one for the EF-Tu:GTP complex and and one for the GTP molecule.

In the case of EF-Tu:GTP complex simulation, the major aim is to comprehend the structural and dynamic properties of the EF-Tu:GTP complex especially those related to the GTPase activity of the protein. Moreover, another aim of this simulation is to analyze the conformational changes in the active site of the protein to sample reactive conformers for the coupled potential (QM/MM) studies.

On the other hand, MD simulation of the GTP molecule is performed in order to investigate the dynamics of GTP molecule in water clusters in the presence of magnesium ion.

4.2.1. Molecular Dynamics Simulations of EF-Tu

15 ns of MD simulation is performed for studying the dynamics of EF-Tu:GTP complex in water clusters. Before analyzing the dynamical features of the individual components of the protein a root mean square deviation (RMSD) calculation is done in order to assess the statistical convergence of the simulation. The C_α atoms of the backbone of the protein are used for the calculation of the RMSD values using the initial geometry as the reference for the positions of C_α atoms. The results displayed 3 ns equilibration period preceding the 12 ns of sampling period in which the RMSD values remain roughly constant with increasing sampling (Figure 4.25). In the light of these results, the following calculations and observations are performed on the sampling period of the simulation in order to avoid the inclusion of misguiding information in the equilibration period.

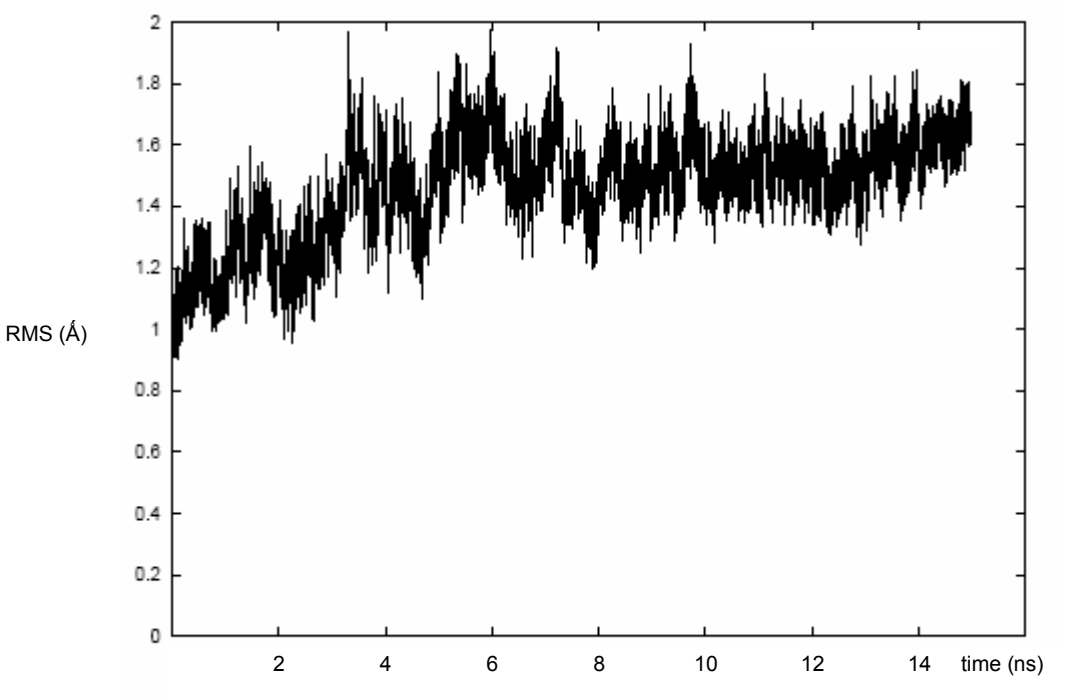

Figure 4.25. RMDS graph of EF-Tu:GTP complex simulation

The major observations of the MD simulation of EF-Tu are related to the motion of the Switch 1 region located in Domain 1 and to the motion of D51 residue of the magnesium ion coordinating network.

During the simulation two different conformations of the Switch 1 region are observed; a contracted form and an elongated form (Figure 4.26). The contracted form of Switch 1 is very similar to the one in the X-ray crystal form.

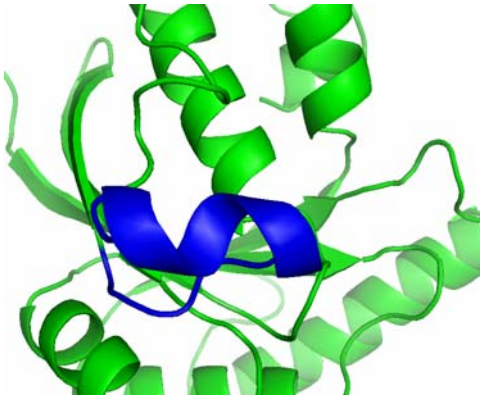

Figure 4.26. Elongated form of switch 1 region

On the other hand, the elongated form displays a distorted form the A" helix in Switch 1 region which may be a signal preceding the GTP hydrolysis. The graph of the evolution of distance between the center of C_α of residues 54-55 and the center of C_α of residues 58-60 (Figure 4.27) displays these conformations of the A" helix clearly. In the contracted form the distance (defined as above) oscillates around 6.7 Å whereas the oscillation is around 9.5 Å in the elongated form.

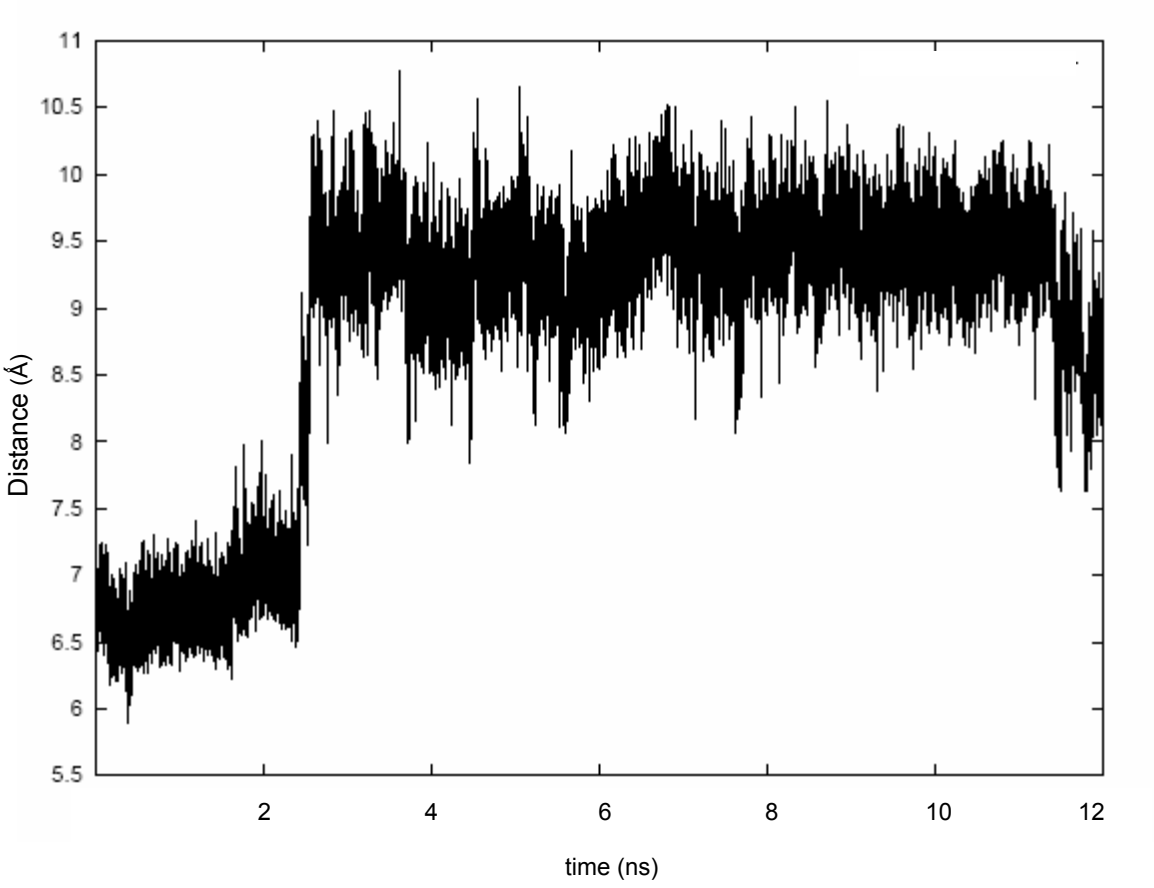

Figure 4.27. Distance vs time graph of switch 1 region

Another important observation from the EF-Tu simulation is the motion of D51 residue that is involved in the Mg^{+2} coordination indirectly by making H-bonds to the both T62 residue and a water molecule in the Mg^{+2} coordination shell (Figure 4.28-29).

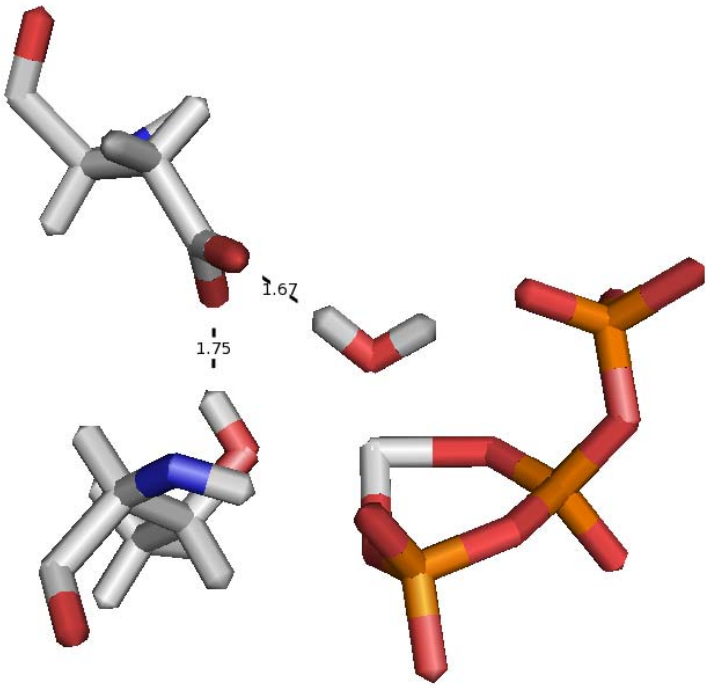

Figure 4.28. D51 H-bonds with T62 and H_2O (close)

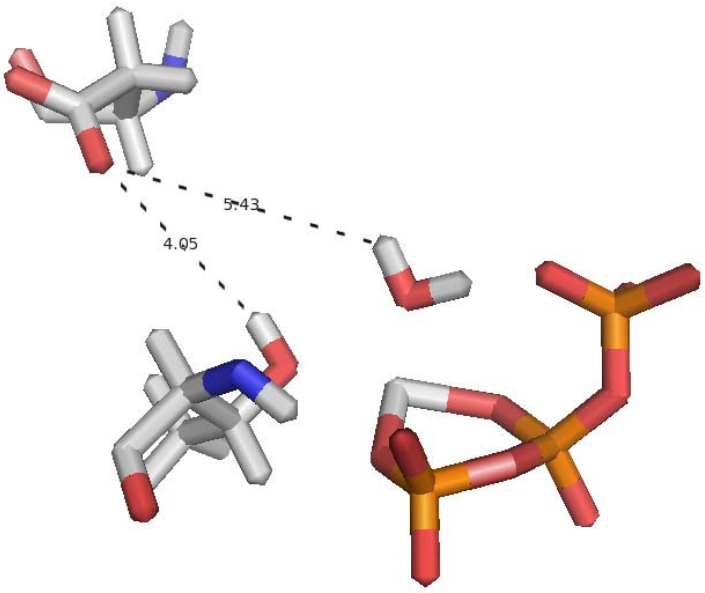

Figure 4.29. D51 H-bonds with T62 and H_2O (away)

The motion of D51 during the trajectory is traced by following the distance of the carboxylate carbon of D51 and the hydrogen atom of the hydroxyl group of T62 (Figure 4.30). The results indicate the presence of two different conformations of D51; one close to the T61 residue like the one in the X-ray crystal structure and other away from it.

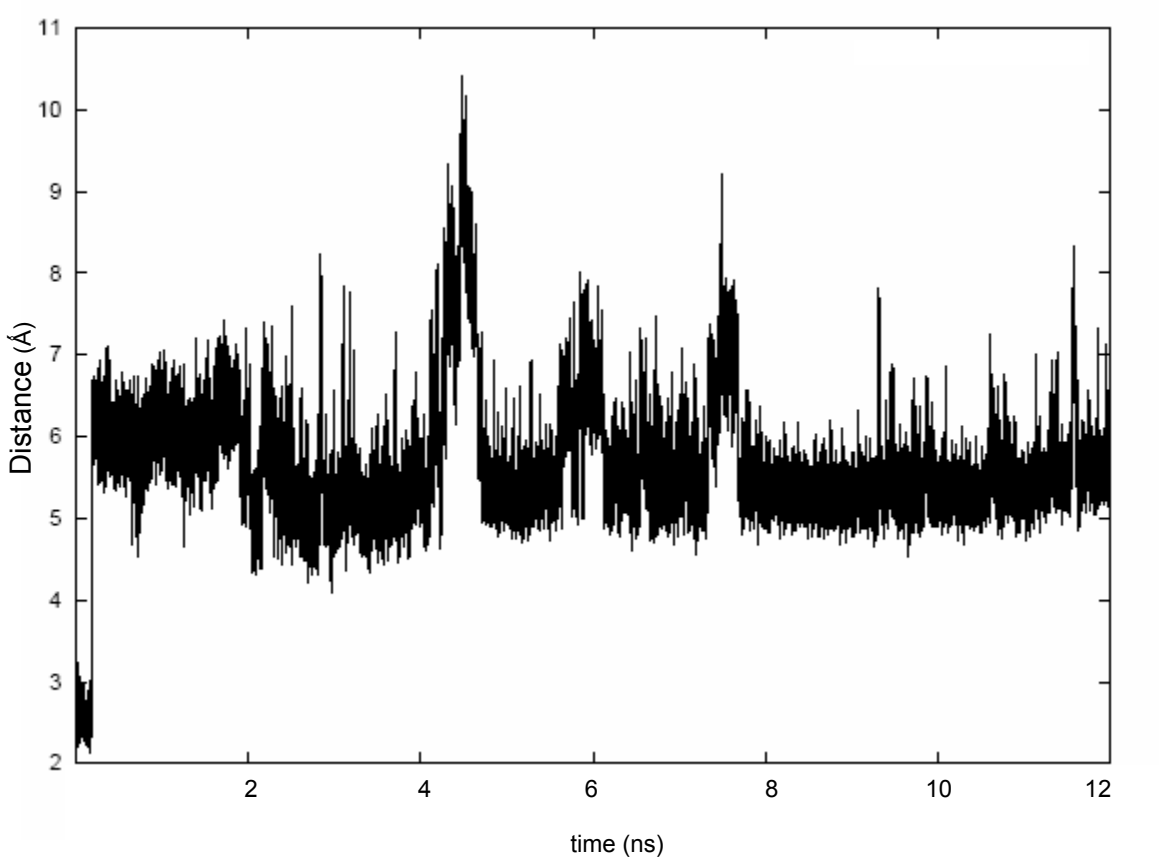

Figure 4.30. Distance vs time graph of D51 and T62

While D51 shows relatively high mobility during the trajectory, the other components forming the Mg^{+2} coordination complex remains essentially immobile. In addition to this, probably the most interesting observation is the correlation between the motions of the D51 residue and the Switch 1 region. When D51 is close to the T62 residue, the Switch 1 region is in the contracted form whereas when D51 is away from the T62 residue Switch 1 is in the elongated form. Moreover, it is known that T62, also a member of Switch 1 region, is bound to Mg^{+2} weaker than its symmetric partner T25 as it will move 4.3 Å away from Mg^{+2} upon GTP hydrolysis due to the conformational change in Switch 1 region. Taking all these into account, the motion of D51 could explain the weaker binding

of T62 to Mg^{+2} compared to T25 and it could be suggested to have a role in the elongation of the Switch 1 region and signal relay preceding the GTP hydrolysis.

Apart from these, H85 residue stays away from the active site and towards the solvent throughout the trajectory (Figure 4.31). In relation to this, the water molecule involved in phosphate hydrolysis stays in an unfavourable position for nucleophilic attack with a hydrogen bond to the backbone amide group of H85. It should be noted here that it is probable to observe the rotation of H85 in a longer simulation and the possibility of H85 rotation can't be ruled out based on the observations of one simulation of 12 ns time span.

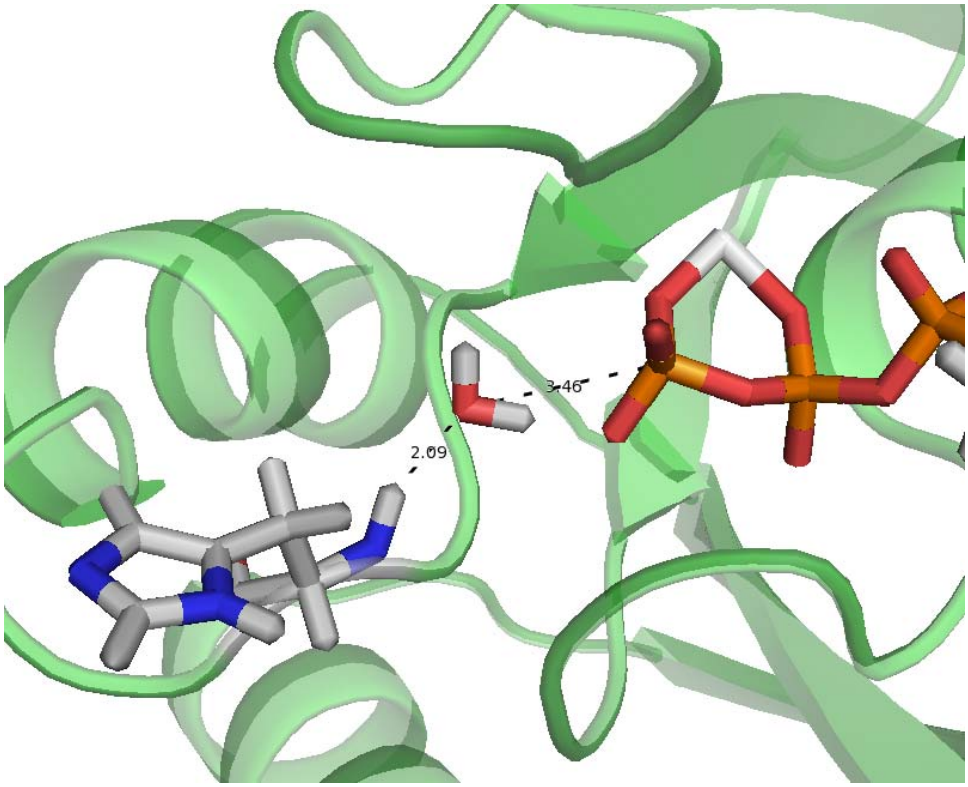

Figure 4.31. H85 in solvent exposed configuration

In the light of these observations and the available mutational data, the role of H85 might be the correct positioning of the water molecule for the nucleophilic attack. In this model, H85 rotates into the active site very rarely in the absence of programmed ribosomes which corresponds to the intrinsic GTPase activity whereas the programmed ribosomes induce the rotation of H85 to the active site catalyzing the GTP hydrolysis reaction.

Moreover, the GTP hydrolysis reaction may be following two different mechanisms in the intrinsic and ribosome induced pathways. For instance, H85 might not be involved in the GTP hydrolysis reaction in the intrinsic GTPase activity while having a crucial catalytic role in the ribosome induced GTPase activity. These two different models could explain both the theoretical and experimental results on the intrinsic and ribosome induced GTPase activity of EF-Tu.

Another residue related to H85 is D87 that was suggested to activate H85 in a general base mechanism for abstracting a proton from the attacking H_2O molecule. H85 side chain is not located in the active site during the simulation but D87 residue displays one close and one away conformation in relation to H85 as suggested in general base mechanism. The graph of distance between the center of carboxylate oxygens of D87 and the H atom on the imidazole ring of H85 (Figure 4.32) reveals the presence of these two conformations but it should be noted that even in the close conformation D21 is not close enough to H85 for activation so that these observations can not be used to support a general base mechanism for GTP hydrolysis on EF-Tu.

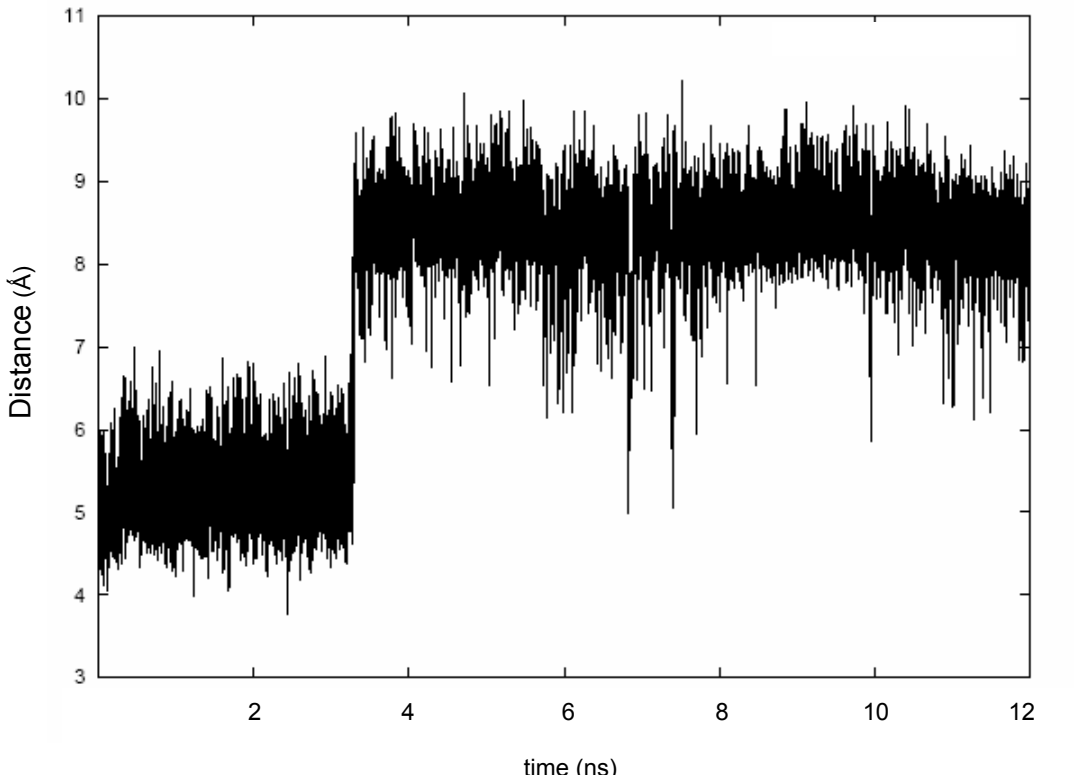

Figure 4.32. Distance vs time graph of D87 and H85

5. CONCLUSIONS

In this study, the hydrolysis of methyl pyrophosphate trianion is modelled by using quantum mechanical methods in order to explore the basic featues of the phosphate hydrolysis reaction.

The hydrolysis reaction of methyl pyrophosphate trianion in the presence of Mg^{+2} ion is modelled by solvent optimizations to comprehend the solvation effects properly during the course of the reaction. The results show that the minimum energy pathway follows a dissociative transition state that is approximately 10 kcal/mol more favorable than the associative pathways when free energies are compared. Moreover, the investigation of the unimolecular dissociation of methyl pyrophosphate trianion demonstrated that the reaction barrier increases with increasing dielectric of the environment and increases in the presence of the Mg^{+2} ion.

Furthemore, the analysis of the physicochemistry of the methyl pyrophosphate trianion hydrolysis reaction yielded the observation that the presence of the Mg^{+2} ion increases the charge transfer interactions favoring nucleophilic participation whereas the absence of the Mg^{+2} ion leads to the dominance of elecrostatic interactions over charge transfer interactions thus favoring a unimolecular dissocation path.

Also, a closer examination of the reaction coordinate reveals that the reaction coordinate can be divided into a physical part, that involves the proper alignment of the attacking water molecule, and a chemical part, that involves the bond formation between the attacking water molecule and the phosphate group. The quantitative analysis illustrates that the physical part of the hydrolysis reaction requires approximately 6 kcal/mol energy that is equivalent to the cost of the proper alignment of the attacking water molecule in the hydrolysis reaction.

In addition to these, the GTP form of Elongation Factor Tu (EF-Tu) is investigated by means of molecular dynamics simulations in order to observe the structural properties of EF-Tu and the possible configurations of the significant residues (D51, T62, H85 etc.) on EF-Tu.

The analysis of the simulations indicate that Aspartate 51 (D51), a residue important in Mg^{+2} ion coordination, is mobile and its movement is correlated with the elongation of the Switch 1 region which shows large conformational change upon GTP hydrolysis reaction on EF-Tu. This coupled movement could be a signal for the GTP hydrolysis reaction on EF-Tu but further studies are needed for a definitive conclusion.

Moreover, Histidine 85 (H85) a catalytically important residue for the ribosome induced GTP hydrolysis reaction stays away from the active site of the EF-Tu throughout the simulation. The role of H85 could be simply the proper alignment of the attacking water molecule, based on the results of the investigation of the reaction coordinate of the methyl pyrophosphate trianion, as this function would correspond to a four orders of magnitude increase in reaction rate compared to a five orders of magnitude increase in reaction rate in ribosome induced GTP hydrolysis.

6. SUGGESTIONS FOR FUTURE WORK

The following suggestions can be made for future work:

- Modelling the hydrolysis reaction of methyl pyrophophate dianion
- QM/MM calculations on the intrinsic GTP hydrolysis of EF-Tu (in progress)
- Molecular dynamics simulations of EF-Tu on ribosome
- Extension of the present molecular dynamics simulations of EF-Tu:GTP complex

REFERENCES

1. Krab, I. M. and A. Parmeggiani, "EF-Tu, A GTPase Odyssey", *Biochimica et Biophysica Acta*, 1443, 1-22, 1998.

2. Polekhina, G.; Thirup, S.; Kjeldgaard, M.; Nissen, P.; Lippmann, C. and J. Nyborg, "Helix Unwinding in the Effector Region of Elongation Factor EF-Tu-GDP", *Structure*, 4 (10), 1141-1151, 1996.

3. Kjeldgaard, M. *et al.*, "The crystal structure of elongation factor EF-Tu from Thermus aquaticus in the GTP conformation", *Structure*, 1, 35–50, 1993.

4. Nissen, P. *et al.*, "The crystal structure of Cys-tRNA^{Cys}:EFTu:GDPNP reveals general and specific features in the ternary complex and in tRNA", *Structure*, 7, 143–156, 1999.

5. Krab, I. M. and A. Parmeggiani, "Mechanisms of EF-Tu, A Pioneer GTPase", *Progress in Nucleic Acid Research and Molecular Biology*, 71, 513-551, 2002.

6. Andersen, G. R.; Nissen, P. and J. Nyborg, "Elongation Factors in Protein Biosynthesis", *Trends in Biochemical Sciences*, 28 (8), 434-441, 2003.

7. Spirin, A. S. "Ribosome as a Molecular Machine", *FEBS Letters,* 514, 2-10, 2002.

8. Song, H.; Parsons, M. R.; Rowsell, S.; Leonard, G. and S. E. V. Philips, "Crystal Structure of Intact Elongation Factor EF-Tu from Escherichia coli in GDP Conformation at 2.05 Å Resolution", *J. Mol. Bio.*, 285, 1245-1256, 1999.

9. Ahmadian, M. R.; Kreutzer, R.; Blechschmidt, B. and M. Sprinzl, "Site Directed Mutagenesis of Thermus Thermophilus EF-Tu: The Substitution of Threonine 62 by Serine and Alanine", *FEBS Letters*, 377, 253-257, 1995.

10. Krab, I. M. and A. Parmeggiani, "Mutagenesis of Three Residues, Isoleucine-60, Threonine-61, and Aspartic Acid-80, Implicated in the GTPase Activity of Escherichia coli Elongation Factor Tu", *Biochemistry*, 38, 13035-13041, 1999.

11. Scarano, G.; Krab, I. M.; Bocchini, V. and A. Parmeggiani, "Relevance of Histidine 84 in the Elongation Factor Tu GTPase Activity and in Poly(Phe) Synthesis: Its Substitution by Glutamine and Alanine", *FEBS Letters*, 365, 214-218, 1995.

12. Daviter, T.; Wieden, H. J. and M. V. Rodnina, "Essential Role of Histidine 84 in Elongation Factor Tu for the Chemical Step of GTP Hydrolysis on the Ribosome", *J. Mol. Bio.*, 332, 689-699, 2003.

13. Jacquet, E. and A. Parmeggiani, "Substitution of Val20 by Gly in elongation factor Tu. Effects on the interaction with elongation factors Ts, aminoacyl-tRNA and ribosomes", *Eur. J. Biochem.* 185**,** 341-346, 1989.

14. Knudsen, C. R. and B. F. C. Clark, "Site Directed Mutagenesis of Arg58 and Asp86 of Elongation Factor Tu From Escherichia coli: Effects on the GTPase Reaction and Aminoacyl-tRNA Binding", *Protein Engineering*, 8 (12), 1267-1273, 1995.

15. Wolfenden, R., "Degrees of Difficulty of Water Consuming Reactions in the Absence of Enzymes", *Chem. Rev.*, 106, 3379-3396, 2006.

16. Kötting, C. and K. Gerwert, "Time Resolved FTIR Studies Provide Acivation Free Energy, Activation Enthalpy and Activation Entropy for GTPase Reactions", *Chemical Physics*, 307, 227-232, 2004.

17. Åqvist, J.; Kolmodin, K.; Florian, J. and A. Warshel, "Mechanistic Alternatives in Phosphate Monoester Hydrolysis: What Conclusions Can Be Drawn From Available Experimental Data", *Chemistry & Biology*, 6 (3), 71-80, 1999.

18. Hu, C. H. and T. Brinck, "Theoretical Studies of the Hydrolysis of the Methyl Phosphate Anion", J. Phys. Chem. A, 103, 5379-5386, 1999.

19. Bianciotto, M.; Barthelat, J. C. and A. Vigroux, "Reactivity of Phosphate Monoester Monoanions in Aqueous Solution 1. Quantum Mechanical Calculations Support the Existence of "Anionic Zwitterion" $MeO^{+}(H)PO_3^{2-}$ as a Key Intermediate in the Dissociative Hydrolysis of the Methyl Phosphate Anion", *J. Am. Chem. Soc.*, 124, 7573-7587, 2002.

20. Wang, Y. N.; Topol, I. A.; Collins, J. R. and S. K. Burt, "Theoretical Studies on the Hydrolysis of Mono-Phosphate and Tri-Phosphate in Gas Phase and Aqueous Solution", *J. Am. Chem. Soc.*, 125, 13265-13273, 2003.

21. Klåhn, M.; Rosta, E. and A. Warshel, "On the Mechanism of Hydrolysis of Phosphate Monoesters Dianions in Solutions and Proteins", *J. Am. Chem. Soc.*, 128, 15310-15323, 2006.

22. Mercero, J. M.; Barrett, P.; Lam, C. W.; Fowler, J. E.; Ugalde, J. M. and L. G. Pedersen,. "Quantum Mechanical Calculations on Phoshate Hydrolysis Reactions", *J. Comp. Chem.*, 21 (1), 43-51, 2000.

23. Franzini, E.; Fantucci, P. and L. D. Gioia, "Density Functional Theory Investigation of Guanosine Triphosphate Models: Catalytic Role of Mg^{+2} Ions In Phosphate Ester Hydrolysis", *Journal of Molecular Catalysis A:Chemical*, 204-205, 409-417, 2003.

24. Akola, J. and R. O. Jones, "ATP Hydrolysis in Water – A Density Functional Study", *J. Phys. Chem. B*, 107, 11774-11783, 2003.

25. Maegley, K. A.; Admiraal, S. J. and D. Herschlag, "Ras – Catalyzed Hydrolysis of GTP: A New Perspective From Model Studies", *Proc. Natl. Acad. Sci. USA*, 93, 8160-8166, 1996.

26. Topol, I. A.; Cachau, R. E.; Nemukhin, A. V.; Grigorenko, B. L. And S. K. Burt, "Quantum Chemical Modelling of the GTP Hydrolysis by the RAS-GAP Protein Complex", *Biochimica et Biophysica Acta*, 1700, 125-136, 2004.

27. Li, G. and X. C. Zhang, "GTP Hydrolysis Mechanism of Ras–like GTPases", *J. Mol. Biol.*, 340, 921-932, 2004.

28. Glennon, T. M.; Villå, J. and A. Warshel, "How Does GAP Catalyze the GTPase Reaction of Ras?: A Computer Simulation Study", *Biochemistry*, 39, 9641-9651, 2000.

29. Cavalli, A. and P. Carloni, "Enzymatic GTP Hydrolysis: Insights From an Ab Initio Molecular Dynamics Study", *J. Am. Chem. Soc.*, 124, 3763-3768, 2002.

30. Grigorenko, B. L.; Nemukhin, A. V.; Topol, I. A.; Cachau, R. E. and S. K. Burt, "QM/MM Modeling the Ras-GAP Catalyzed Hydrolysis of Guanosine Triphosphate", *Proteins: Structure, Function, and Bioinformatics*, 60, 495-503, 2005.

31. Wittinghofer, A., "Phosphoryl Transfer in Ras Proteins, Conclusive or Elusive", *Trends in Biochemical Sciences*, 31 (1), 20-23, 2006.

32. Parr, R. G. and W. Yang, *Density Functional Theory of Atoms and Molecules*, Oxford University Press, New York, 1989.

33. Handy, N. C., "Density Functional Theory", in: B. O. Roos (ed.), *Lecture Notes in Quantum Chemistry*, 2, 91-123, Springer-Verlag, Berlin, 1994.

34. Frisch, *et al.*, *Gaussian 03 Revision D.01*, Gaussian, Inc., Wallingford CT, 2004.

35. Leach, A. R., *Molecular Modelling Principles and Applications*, Prentice Hall, England, 2001.

36. Becke, A. D., "Density-Functional Exchange Energy Approximation with Correct Asymptotic Behavior", *Phys. Rev. A*, 38, 3098-3103, 1988.

37. Becke, A. D., "A New Mixing of Hartree-Fock and Local Density Functional Theories", *J. Chem. Phys.*, 38, 1372-1377, 1993.

38. Lee, C.; W. Yang and R. G. Parr, “Development of Colle-Salvetti Correlation Energy Formula into a Functional of The Electron Density”, *Phys. Rev. B*, 37, 785-789, 1988.

39. Becke, A. D., “Density Functional Thermochemistry. III. The Role of Exact Exchange”, *J. Chem. Phys.*, 98, 5648-5652, 1993.

40. Pauling, L. J., “The Nature of the Chemical Bond. IV. The Energy of Single Bonds and the Relative Electronegativity of Atoms”, *J. Am. Chem. Soc.*, 54, 3570-3582, 1932.

41. Zhao, Y. and D. G. Truhlar, “Hybrid Meta Density Functional Theory Methods for Thermochemistry, Thermochemical Kinetics, and Noncovalent Interactions: The MPW1B95 and MPWB1K Models and Comparative Assessments for Hydrogen Bonding and van der Waals Interactions”, *J. Phys. Chem. A*, 108, 6908-6918, 2004.

42. Perdew, J. P., *Electronic Structure of Solids*, Ziesche, P. and H. Eschig, Eds.; Akademie Verlag, Berlin, 1991.

43. Becke, A. D., “Density Functional Thermochemistry. IV. A New Dynamical Correlation Functional and Implications For Exact Exchange Mixing”, *J. Chem. Phys.*, 104 (3), 1040-1046, 1996.

44. Cossi, M., Rega, N., Scalmani, G. and V. Barone, “Energies, Structures, and Electronic Properties in Solution with the C-PCM Solvation Model”, *J. Comp. Chem.*, 24 (6), 669-681, 2002.

45. Tomasi, J.; M. Benedetta and R. Cammi, “Quantum Mechanical Continuum Solvation Models”, *Chem. Rev.*, 105, 2999-3093, 2005.

46. Cancès, E.; M. Benedetta and J. Tomasi, “Evaluation of Solvent Effects in Isotropic and Anisotropic Dielectrics and in Ionic Solutions with a Unified Integral Equation Method: Theoretical Bases, Computational Implementation, and Numerical Applications”, *J. Phys. Chem. B*, 101, 10506-10517, 1997.

47. Cancès, E.; M. Benedetta and J. Tomasi, "A New Integral Equation Formalism for the Polarizable Continuum Model: Theoretical Background and Applications to Isotropic and Anisotropic Dielectrics", *J. Chem. Phys.*, 107, 3032-3041.1997.

48. Cramer, C. J., *Essentials of Computational Chemistry: Theories and Models*, 2nd ed., John Wiley & Sons Ltd., USA, 2004.

49. Meagher, K. L., L. T. Redman and H. A. Carlson, "Development of Polyphosphate Parameters for Use with the AMBER Force Field", *J. Comp. Chem.*, 24, 1016-1025, 2003.

50. D. A. Case, T. A. Darden, T. E. Cheatham, III, C. L. Simmerling, J. Wang, R. E. Duke, R. Luo, K. M. Merz, B. Wang, D. A. Pearlman, M. Crowley, S. Brozell, V. Tsui, H. Gohlke, J. Mongan, V. Hornak, G. Cui, P. Beroza, C. Schafmeister, J. W. Caldwell, W. S. Ross, and P. A. Kollman, *AMBER 8 Program Package,* University of California, San Francisco, 2004.